Article

Differentiation fate of a stem-like CD4 T cell controls immunity to cancer

https://doi.org/10.1038/s41586-024-08076-7

Received: 4 December 2023

Accepted: 18 September 2024

Published online: 23 October 2024

Check for updates

Maria A. Cardenas[1], Nataliya Prokhnevska[1], Ewelina Sobierajska[1], Petra Gregorova[1], Christopher B. Medina[2], Rajesh M. Valanparambil[2], Rachel Greenwald[1], Luke DelBalzo[1], Mehmet Asim Bilen[2,3], Shreyas S. Joshi[1,4], Vikram M. Narayan[1,4], Viraj A. Master[1,4], Martin G. Sanda[1,4] & Haydn T. Kissick[1,2,4,5] ✉

The T cell response to cancer controls disease progression and response to immunotherapy[1–3]. Despite extensive knowledge regarding CD8 T cells, how CD4 T cells contribute to this process is less well understood. Here we identified a population of PD1$^+$TCF1$^+$ CD4 T cells with stem-like properties that are capable of self-renewal and differentiation into canonical CD4 effector cells. Primarily residing in tumour-draining lymph nodes (TDLNs), these tumour-specific CD4 T cells are restricted by T regulatory (T_{reg}) cells to a stem-like fate that predominantly generated induced T_{reg} (iT_{reg}) cells, limiting effector CD8 T cell responses to the tumour. By contrast, upon T_{reg} depletion, stem-like CD4 T cells differentiated into T helper 1 (T_H1) cells, and via IFNγ production induced robust effector differentiation from TCF1$^+$ CD8 T cells in TDLNs, a state we defined as 'active'. Notably, enforcing TBET expression in transferred stem-like CD4 T cells was sufficient to overcome the established restricted T cell state. Despite the presence of T_{reg} cells, endogenous stem-like CD4 T cells actively generated T_H1 cells, which were required to restore TDLN effector CD8 T cell differentiation, enhance tumour control and rescue response to immunotherapy. In agreement, T_H1 differentiation in patients with kidney cancer predicted successful immunotherapy responses and improved progression-free survival. Together, these findings identify a stem-like CD4 T cell population that through alternative differentiation fates controls the switch between restricted and active T cell states with implications for cancer immunotherapies.

CD4 T cells are associated with successful immunotherapy responses, adoptive T cell therapies, and vaccination strategies across cancer types[4,5]. The expansion of conventional CD4 T cells following checkpoint therapy, or their presence in tertiary lymphoid structures often predicts favourable clinical outcomes[4,6–9]. Moreover, the differentiation of CD4 T cells into T_H1 or T follicular helper (T_{FH})-like subsets appears to be critical for effective tumour control[10–14]. However, CD4 T cells can also be found as T_{reg} cells or dysfunctional phenotypes, and these states are frequently associated with disease progression[5,15,16]. Thus, although activated CD4 T cells are a significant component of the cancer immune response, the mechanisms that determine whether CD4 T cell subsets will enhance anti-tumour immunity or contribute to tumour progression remain poorly understood. Here we examine the differentiation fate of tumour-specific CD4 T cells to better understand their functional roles in the anti-tumour response.

PD1$^+$TCF1$^+$lin$^-$ CD4 T cells infiltrate tumours

To examine the heterogeneity of the CD4 T cell response, we first performed single-cell RNA sequencing (scRNA-seq) on PD1$^+$CD45RA$^-$ CD4 T cells infiltrating human kidney tumours. We identified three clusters that expressed genes related to antigenic stimulation and tissue migration (Fig. 1a and Extended Data Fig. 1a,b). Cluster 1 cells had a T_{reg} phenotype (expressing *FOXP3* and *IL2RA*) and were significantly enriched for a T_{reg} signature (Fig. 1b and Extended Data Fig. 1b,c). Cluster 2 cells expressed *EOMES* and various cytotoxic molecules, with minimal *TBX21* (encoding TBET) expression or enrichment for a T_H1 signature (Fig. 1b and Extended Data Fig. 1b,c). Notably, cluster 3 cells did not express any of the major lineage-defining transcription factors (*BCL6*, *TBX21*, *GATA3* or *RORC*). These CD4 T cells instead expressed high levels of *TCF7* (Fig. 1b), genes related to the stem cell programme, and low expression of genes encoding inhibitory receptors and effector molecules (Extended Data Fig. 1b). Furthermore, *TCF7*-expressing CD4 T cells were significantly enriched for a human stem-like CD8 T cell gene signature[17] (Fig. 1c) and had the lowest enrichment score for cell proliferation and CD4 helper signatures, suggesting a more quiescent state (Extended Data Fig. 1c and Supplementary Table 4).

We extended these findings to 125 kidney, 17 bladder and 6 prostate tumours using flow cytometry. We found a wide range of CD4 T cell infiltration between patients and cancer types, with most cells

[1]Department of Urology, Emory University School of Medicine, Atlanta, GA, USA. [2]Emory Vaccine Center, Emory University School of Medicine, Atlanta, GA, USA. [3]Department of Hematology and Medical Oncology, Emory University School of Medicine, Atlanta, GA, USA. [4]Winship Cancer Institute of Emory University, Atlanta, GA, USA. [5]Department of Microbiology and Immunology, Emory University School of Medicine, Atlanta, GA, USA. ✉e-mail: haydn.kissick@emory.edu

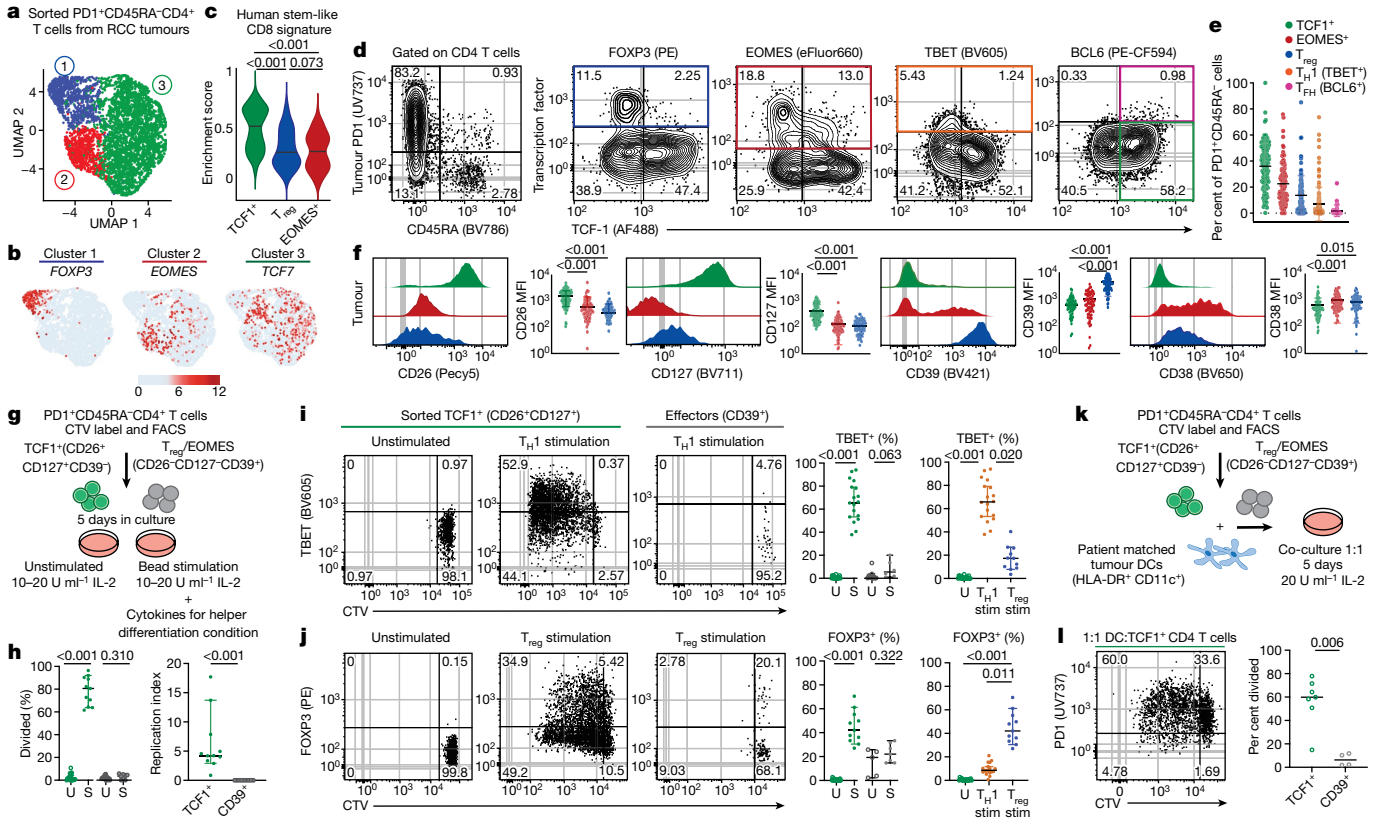

Fig. 1 | PD1$^+$TCF1$^+$ stem-like CD4 T cells are the predominant population in human tumours and TDLNs. a, scRNA-seq of sorted tumour PD1$^+$CD45RA$^-$ CD4 T cells from patients with renal cell carcinoma (RCC) ($n = 2$). **b**, Normalized expression of transcription factors that define each cluster. **c**, VISION gene set enrichment analysis (GSEA) using the human cancer stem-like CD8 T cell signature. Enrichment scores are shown as violin plots; horizontal bars show the mean; one-way analysis of variance (ANOVA) with Tukey's multiple-comparison test. **d**–**f**, Representative flow cytometry phenotype (**d**) and frequency (**e**) of activated (PD1$^+$CD45RA$^-$) CD4 T cell populations in kidney tumours, and expression of selected markers (**f**). Data are mean ± s.d.; Kruskal–Wallis test with Dunn's multiple-comparison test ($n = 125$ patients with kidney cancer). MFI, geometric mean fluorescence intensity. **g**, Experimental design to test the proliferative and differentiation capacity of TCF1$^+$lin$^-$ and CD39$^+$ CD4 T cells from primary tumours. **h**, Frequency and replication index of sorted TCF1$^+$lin$^-$ ($n = 11$) or CD39$^+$ ($n = 9$) CD4 T cells after five days under unstimulated (U) or stimulated (S) T_H0 conditions. Data are median ± 95% confidence interval; two-sided unpaired Mann–Whitney U test. **i**,**j**, Representative plot showing CTV dilution and expression of TBET and FOXP3 transcription factors after five days in unstimulated, T_H1 (**i**) or T_{reg} (**j**) stimulating (stim) conditions (T_H1 stimulation, $n = 18$; T_{reg} stimulation, $n = 11$). Data are median ± 95% confidence interval; two-sided unpaired Mann–Whitney U test when comparing U versus S within the same population; Kruskal–Wallis test with Dunn's multiple-comparison tests for comparing three groups. **k**, Experimental design for dendritic cell (DC) and PD1$^+$ CD4 T cell co-cultures. **l**, Representative plot of sorted TCF1$^+$lin$^-$ CD4 T cells after 5 days of 1:1 co-culture with donor-matched dendritic cells ($n = 7$ patients for TCF1$^+$lin$^-$ and $n = 4$ patients for CD39$^+$). Medians shown and analysed by two-sided unpaired Mann–Whitney U test.

expressing PD1 (Fig. 1d and Extended Data Fig. 1d,e). In agreement with the scRNA-seq analysis, around 35% of activated (PD1$^+$CD45RA$^-$) CD4 T cells expressed FOXP3 or EOMES, with very few cells expressing TBET or BCL6 in most patients with kidney cancer (Fig. 1d,e and Extended Data Fig. 1f). The remaining tumour CD4 T cells were negative for lineage-defining transcription factors, expressed TCF1 and various co-stimulatory molecules and cytokine receptors, and were consistently the most frequent PD1$^+$ population (Fig. 1d–f and Extended Data Fig. 1f–h). Furthermore, despite their activated state, these cells were negative for effector molecules and inhibitory receptors (Fig. 1f and Extended Data Fig. 1g,h). By contrast, FOXP3$^+$ and EOMES$^+$ cells expressed CD39 and molecules associated with their respective phenotypes (Fig. 1f and Extended Data Fig. 1g,h).

Finally, we examined the phenotype of CD4 T cells in non-metastatic TDLNs from 12 patients with kidney cancer. We found 20–60% of the total CD4 T cell pool in a PD1$^+$CD45RA$^-$ activated state, with TCF1$^+$ lineage-negative (lin$^-$) CD4 T cells being the most frequent population (Extended Data Fig. 1i–k). These cells expressed similar patterns of co-stimulatory molecules, cytokine receptors, and effector molecules as the TCF1$^+$lin$^-$ CD4 T cells found in the tumour (Extended Data Fig. 1j–l). Together, these data identified a TCF1$^+$lin$^-$ population as the most dominant cell in the PD1$^+$ CD4 T cell pool in tumours and TDLNs across various human cancer types.

TCF1$^+$lin$^-$ cells are precursors of CD4 helpers

We next tested the proliferative capacity of these cells by sorting cell trace violet (CTV)-labelled TCF1$^+$lin$^-$ or CD39$^+$ CD4 T cells from primary kidney tumours (Supplementary Data 1a) and cultured them in vitro for five days under unstimulated (U) or stimulated (S) T_H0 conditions (Fig. 1g and Methods). Upon stimulation, TCF1$^+$lin$^-$ CD4 T cells underwent extensive proliferation and retained their activated but uncommitted phenotype, whereas CD39$^+$ cells remained undivided (Fig. 1h and Extended Data Fig. 2a,b).

The lack of lineage transcription factor expression, concomitant with prior studies finding plasticity among CD4 lineages[18,19], prompted us to investigate whether TCF1$^+$lin$^-$ cells could differentiate to canonical CD4 effector programmes. PD1$^+$TCF1$^+$lin$^-$ or CD39$^+$ CD4 T cells were sorted from human tumours as described above and cultured in cytokine polarization conditions towards T_H1, T_{reg}, T_{FH} or EOMES lineages. TCF1$^+$lin$^-$ CD4 T cells downregulated TCF1 and upregulated TBET and GZMB in response to T_H1 cell polarization (Fig. 1i and Extended

Data Fig. 2c), whereas they upregulated FOXP3 and CD25 in response to T_{reg} cell polarization (Fig. 1j and Extended Data Fig. 2c). TCF1$^+$lin$^-$ CD4 T cells were also capable of upregulating EOMES and BCL6-related programmes, in non-classical T_H1 and T_{FH} polarizing conditions, respectively (Extended Data Fig. 2d–f). It is worth noting that although T_H1 and T_{FH} CD4 T cells were rarely found infiltrating kidney tumours, PD1$^+$TCF1$^+$lin$^-$ CD4 T cells had the capacity to acquire these programmes upon stimulation with the appropriate conditions. By contrast, CD39$^+$ CD4 T cells retained expression of their respective transcription factors and effector molecules in unstimulated conditions and across all stimulated conditions (Fig. 1i,j and Extended Data Fig. 2a–f).

To test whether PD1$^+$TCF1$^+$lin$^-$ CD4 T cells responded to physiological levels of stimulation, we sorted and co-cultured these cells with donor-matched CD11c$^+$ major histocompatibility complex class II (MHCII)-expressing dendritic cells at a 1:1 ratio (Fig. 1k and Supplementary Data 1a). PD1$^+$TCF1$^+$lin$^-$ CD4 T cells underwent extensive proliferation, maintained CD26 expression, and downregulated markers inversely associated with T cell receptor (TCR) stimulation (Fig. 1l and Extended Data Fig. 2g–i). Moreover, upon addition of IL-12 to the co-culture, TCF1$^+$lin$^-$ CD4 T cells upregulated TBET and acquired a T_H1 programme upon division (Extended Data Fig. 2j). By contrast, minimal to no proliferation was observed for co-cultured CD39$^+$ effector CD4 T cells (Extended Data Fig. 2g–i). PD1$^+$CD39$^+$ cells underwent proliferation only upon administration of a high dose of IL-2 (4,000 U ml^{-1}), a dose previously shown to induce effector CD8 T cell proliferation[20] (Extended Data Fig. 2k,l). Together, these results show that despite existing in a quiescent state in vivo, TCF1$^+$lin$^-$ CD4 T cells retain extensive proliferative and differentiation potential into various lineages of CD4 T cells upon stimulation, whereas CD39$^+$ CD4 T cells are in more terminally differentiated states.

The differentiation capacity of TCF1$^+$lin$^-$ CD4 T cells led us to investigate the relationship between CD4 T cell subsets in tumours from patients with kidney cancer using paired scRNA-seq and single-cell TCR sequencing data. Among the clonally expanded TCRs for both patients, we found shared clonal overlap between the TCF1$^+$lin$^-$ population and T_{reg} or EOMES clusters. Additionally, a small number of clones overlapped between all three CD4 subsets (purple) in both patients (Extended Data Fig. 2m,n). These shared TCR clonotypes suggest a lineage relationship between TCF1$^+$lin$^-$ and the T_{reg} cells and EOMES$^+$ CD4 T cells in kidney tumours. Collectively, these data indicate that PD1$^+$TCF1$^+$lin$^-$ CD4 T cells have functional stem-like properties and act as a precursor to other differentiated effector CD4 T cells within human tumours.

TCF1$^+$lin$^-$ CD4 T cells arise within TDLNs

To address antigen specificity, differentiation kinetics and functional relevance of TCF1$^+$lin$^-$ CD4 T cells, we turned to mouse models. We first used TRAMPC1 cells expressing the lymphocytic choriomeningitis (LCMV) glycoprotein (GP) to track the activation and differentiation of antigen-specific (GP66$^+$) CD4 T cells throughout tumour progression. Following inoculation with TRAMPC1-GP, GP66$^+$ CD4 T cells underwent expansion in TDLNs and persisted throughout the five-week response (Fig. 2a and Extended Data Fig. 3a). Notably, the majority of GP66$^+$ CD4 T cells acquired a TCF1$^+$lin$^-$ phenotype in TDLNs within the first week, suggesting CD4 T cells are rapidly skewed towards this activated state (Extended Data Fig. 3a). Five weeks after tumour inoculation, GP66$^+$ CD4 T cells in TDLNs all expressed activation markers and primarily exhibited a TCF1$^+$lin$^-$, FOXP3$^+$ or BCL6$^+$ phenotype, with very few cells expressing TBET, RORγt or EOMES (Fig. 2b and Extended Data Fig. 3b). Phenotypically, GP66$^+$TCF1$^+$lin$^-$ CD4 T cells expressed high levels of the tolerance-associated markers FR4 and CD73 (refs. 15,21,22), regulators of T cell differentiation, and limited expression of effector molecules (Fig. 2c and Extended Data Fig. 3b). In contrast to TDLNs, GP66$^+$ CD4 T cells in tumours were primarily T_{reg} cells, with a smaller proportion of cells retaining a TCF1$^+$lin$^-$ phenotype (Fig. 2a,b and Extended Data Fig. 3c). The high frequency and phenotype of PD1$^+$TCF1$^+$lin$^-$ CD4 T cells was conserved across B16F10-GP, MC38 and both subcutaneous and orthotopic RENCA-HA tumour models (Extended Data Fig. 3d–k). Furthermore, transfer of naive CD4 T cells from SMARTA mice—which express a TCR with specificity for LCMV GP—with a large (500,000) or small (10,000) number of precursors resulted in a similar in vivo differentiation trajectory of antigen-specific CD4 T cells from naive to TCF1$^+$lin$^-$ in mice inoculated with TRAMPC1-GP cells (Extended Data Fig. 4a–i). Seven days post transfer, around 95% of the transferred SMARTA CD4 T cells expressed PD1 and Ki67 and were TCF1$^+$lin$^-$ within TDLNs and tumours (Extended Data Fig. 4b,c). Over the four- to five-week tumour response, 20% and 85% of transferred SMARTA CD4 T cells expressed FOXP3 within TDLNs and tumours, respectively, with minimal expression of TBET, RORγt or BCL6 (Extended Data Fig. 4c–i). Together, these data show the generation of an activated, undifferentiated population of tumour-specific TCF1$^+$lin$^-$ CD4 T cells in TDLNs and tumours and suggest that over time this population can potentially give rise to iT_{reg} cells across mouse cancer models.

To examine the proliferation and differentiation capacity of TCF1$^+$lin$^-$ CD4 T cells to the GP antigen in a different environment, we sorted these cells from TDLNs of 5-week TRAMPC1-GP tumour-bearing mice (Supplementary Data 1b) and transferred them into naive mice that were immediately infected with LCMV Armstrong (Fig. 2d). Eight days after infection, CD45.1$^+$ SMARTA TCF1$^+$lin$^-$ CD4 T cells exhibited more than 20-fold expansion in blood, lymphoid and non-lymphoid organs, with a similar distribution as the endogenous virus-specific GP66$^+$ CD4 T cells (Extended Data Fig. 4j). Notably, TCF1$^+$lin$^-$ SMARTA T cells differentiated into T_H1 and T_{FH} cells in response to LCMV, with minimal T_{reg} differentiation, analogous to endogenous virus-specific CD4 T cells across all tissues examined (Fig. 2e,f and Extended Data Fig. 4j,k). Thus, tumour-specific TCF1$^+$lin$^-$ CD4 T cells have stem-like properties with extensive capacity to proliferate and differentiate into different effector lineages of CD4 T cells depending on their environment. On the basis of these observations, we refer to TCF1$^+$lin$^-$ CD4 cells as 'stem-like' CD4 T cells.

T_{reg} cells inhibit stem-like differentiation to T_H1 cells

Given that stem-like CD4 T cells had the capacity to differentiate into helper CD4 lineages outside the tumour environment, we next investigated potential mechanisms that negatively regulated their differentiation in cancer. First, we examined the role of PD1, given its high expression on stem-like CD4 T cells and its inhibitory mechanisms that regulate differentiation of stem-like to effector CD8 T cells[23–25]. After two weeks of PDL1 blockade therapy, both antigen-specific and bulk PD1$^+$ CD4 T cells maintained a stem-like and T_{reg} phenotype in TDLNs and tumours across refractory TRAMPC1-GP and responsive MC38 and RENCA-HA models (Extended Data Fig. 4l–p), indicating that PD1 does not regulate stem-like CD4 T cell differentiation in cancer.

Our data show that T_{reg} cells make up a large fraction of the PD1$^+$ CD4 T cell pool in TDLNs and tumours, so we next examined whether T_{reg} cells suppress stem-like CD4 T cell differentiation to canonical helper lineages. Indeed, FOXP3$^+$ T_{reg} cell depletion three to four weeks after TRAMPC1-GP tumour inoculation in DEREG mice[12] (denoted as FOXP3-DTR) resulted in significant tumour-specific GP66$^+$ CD4 T cell expansion and T_H1 differentiation in TDLNs and tumours (Fig. 3a–d and Extended Data Fig. 5a–c). Differentiated GP66$^+$ T_H1 CD4 T cells exhibited downregulation of TCF1 and increased expression of TBET and other known T_H1 markers, along with increased production of IFNγ and IL-2 (Fig. 3e and Extended Data Fig. 5a,b). This shift in CD4 T cell differentiation peaked on day 5 and was maintained until day 25 post depletion, despite the return of host T_{reg} cells (Fig. 3c,d and Extended Data Fig. 5b). T_H1 accumulation was not exclusive to the GP66

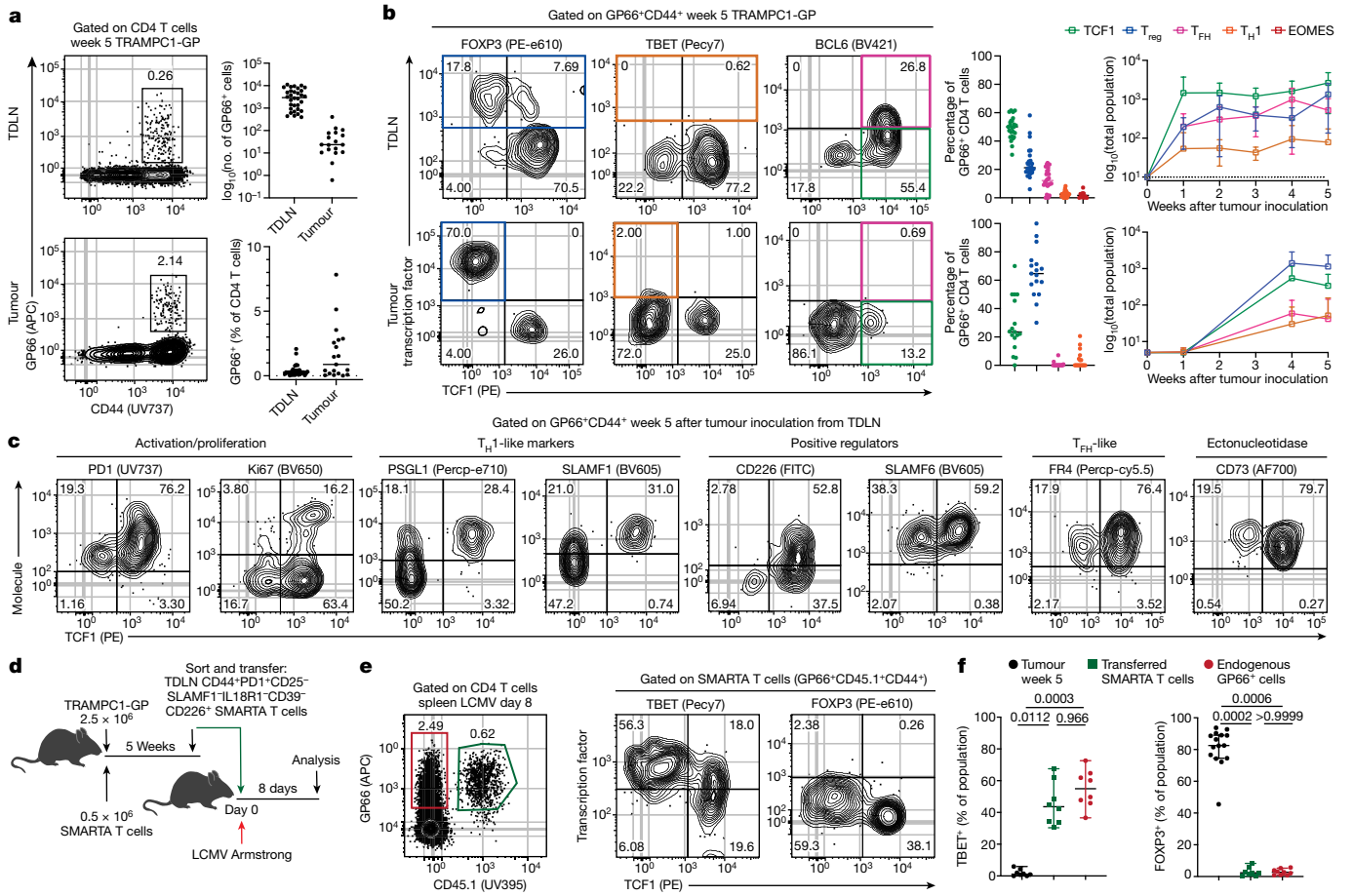

Fig. 2 | Identification of a TCF1$^+$lin$^-$ stem-like CD4 T cell population in mouse cancer models. a, Representative I-A^{b}GP$_{66}$ tetramer staining in TDLNs (top) and tumour (bottom) five weeks after TRAMPC1-GP inoculation. Summary plots show the frequency and number of GP66$^+$ CD4 T cells in each tissue. **b**, Phenotypic analysis of GP66$^+$ CD4 T cells in TDLNs (top) and tumours (bottom) five weeks after TRAMPC1-GP inoculation. Summary plots show the frequency and number of GP66$^+$ CD4 T cells that express the respective lineage transcription factor in each tissue. Data are median or mean ± s.d. ($n > 5$ mice per timepoint). **c**, Phenotypic characterization of GP66$^+$ CD4 T cells in TDLNs of TRAMPC1-GP tumour-bearing mice after five weeks ($n > 5$ mice for each marker). **d**, Experimental design to test the functional capacity of sorted PD1$^+$TCF1$^+$lin$^-$ SMARTA T cells from TDLNs ($n = 40$ pooled mice as donors from 2 independent experiments). **e**, Representative phenotypic analysis of recovered SMARTAs and endogenous I-A^{b}GP$_{66}$ CD4 T cells in the spleen eight days after LCMV Armstrong infection. **f**, Frequency of SMARTA T cells or virus-specific endogenous GP66$^+$ cells expressing TBET and FOXP3. 'Tumour week 5' represents SMARTA T cells in the tumour from donor mice prior to sorting. Data are representative of 2 independent experiments ($n = 8$ recipient mice); median ± 95% confidence interval; Kruskal–Wallis test with Dunn's multiple-comparison tests.

antigen, as bulk PD1$^+$ CD4 T cells were similarly skewed towards the T$_H$1 lineage in TDLNs, blood and tumours across all models (Extended Data Fig. 5c–g).

We next examined the transcriptional changes on stem-like CD4 T cells after T$_{reg}$ depletion, and their relationship to the emerging T$_H$1 cells. We performed scRNA-seq on bulk CD44$^+$PD1$^+$ CD4 T cells from TRAMPC1-GP TDLNs untreated or 5 days after T$_{reg}$ depletion, with naive (CD44$^-$CD62L$^+$) CD4 T cells from lymph nodes included as a control. Transcriptional analysis identified five clusters of activated CD4 T cells, with high expression of markers related to antigen experience (Extended Data Fig. 5h,i). Consistent with our flow cytometry data, stem-like CD4 T cells (cluster 1) were present in both untreated and T$_{reg}$-depleted mice. These cells were characterized by a unique transcriptional profile, with high expression of *Tcf7*, *Slamf6*, *Lef1* and *Gpr183*, and significant enrichment for the chronic LCMV-specific CD4 T cell precursor signature[26] (Extended Data Fig. 5j,k and Supplementary Table 4). Upon T$_{reg}$ depletion, TCF1$^+$lin$^-$ CD4 T cells retained their stem-like programme, but upregulated genes associated with T$_H$1 differentiation (Extended Data Fig. 5l and Supplementary Table 2). In comparison, differentiated T$_H$1 cells (cluster 3) comprised almost exclusively of activated CD4 T cells from T$_{reg}$-depleted mice expressed *Tbx21* and several effector T$_H$1 molecules (Extended Data Fig. 5j–h). Notably, TCRβ sequencing showed that whereas in untreated conditions, stem-like CD4 T cells shared clonality with T$_{reg}$ and T$_{FH}$ populations in TDLNs (Extended Data Fig. 5m), stem-like CD4 T cells from T$_{reg}$-depleted mice shared more than 90% of clonotypes with the clonally expanded T$_H$1 cluster (Fig. 3f). Together, these data indicate that the stem-like CD4 T cell population is a precursor to differentiated T$_H$1 cells in cancer.

To further examine this relationship, we sorted tumour-specific PD1$^+$ SMARTA stem-like or T$_{reg}$ cells from TDLNs of 3-week TRAMPC1-GP tumour-bearing mice (Supplementary Data 1d) and transferred these cells into congenically distinct tumour-matched wild-type or FOXP3-DTR recipients (Fig. 3g). All recipient mice received diphtheria toxin two days after transfer and the phenotype of transferred cells was examined five days later. Transferred stem-like SMARTA T cells underwent a greater expansion in both conditions compared with T$_{reg}$ cells (Fig. 3h) and were primarily found within TDLNs (Extended Data Fig. 6a,b). Phenotypically, stem-like CD4 T cells re-established the stem-like pool in TDLNs, with a small fraction differentiating into T$_{reg}$ and T$_{FH}$ cells in wild-type mice (Fig. 3i and Extended Data Fig. 6a). In T$_{reg}$-depleted mice, stem-like CD4 T cells also re-established the

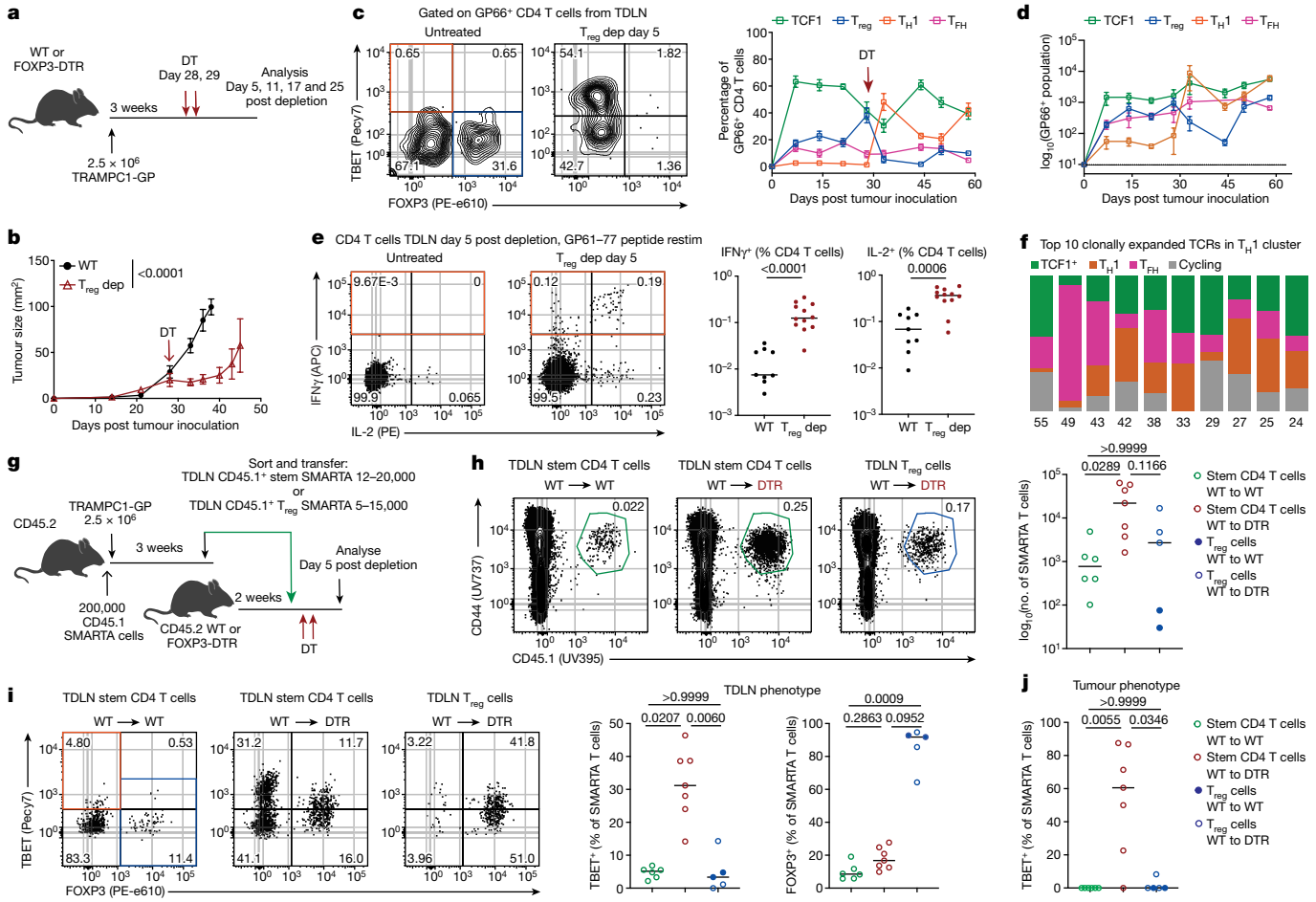

Fig. 3 | Regulatory T cells actively suppress differentiation of stem-like CD4 T cells to T_H1 cells. a, Experimental design. T_{reg} cells were transiently depleted in TRAMPC1-GP tumour-bearing mice after three to four weeks by intraperitoneal administration of diphtheria toxin (DT) on two consecutive days. WT, wild type. **b**, Tumour kinetics shown as mean tumour diameter ± s.e.m in untreated ($n = 10$) or T_{reg}-depleted (dep) ($n = 13$) mice. Analysed by two-sided unpaired Mann–Whitney U test at endpoint. **c**,**d**, Phenotype of GP66$^+$ CD4 T cells in TDLNs of untreated mice or at various timepoints after T_{reg} depletion. Summary plots show the frequency (**c**) or total number (**d**) of GP66$^+$ phenotypes in TDLNs at various timepoints prior to and after T_{reg} depletion. Data are mean ± s.e.m, $n \geq 5$ mice per timepoint. **e**, Representative IFNγ and IL-2 staining after in vitro restimulation (restim) with GP61–77 peptide in CD4 T cells from TDLNs in untreated ($n = 9$) mice or 5 days after T_{reg} depletion ($n = 12$). Data are median; two-sided unpaired Mann–Whitney U test. **f**, Cluster distribution of the ten most dominant TCR clonotypes in the T_H1 cluster from T_{reg}-depleted mice. The number of cells sharing the respective TCR clonotype is indicated below the graph ($n = 4$ mice pooled for sorting). **g**, Experimental design. PD1$^+$ stem SMARTA T cells or T_{reg} SMARTA T cells from TRAMPC1-GP TDLNs were transferred into tumour-matched wild-type or FOXP3-DTR recipients. **h**, Total number of recovered stem SMARTA T cells or T_{reg} SMARTA T cells in wild-type or T_{reg}-depleted mice in TDLNs. **i**,**j**, Phenotype of stem and T_{reg} SMARTA T cells in TDLNs (**i**) and tumours (**j**) after transfer. Data are representative of two independent experiments (25–30 pooled mice for each experiment, $n = 3$ or 4 recipient mice per experiment for each condition). Data are median; Kruskal–Wallis test with Dunn's multiple-comparison tests.

stem-like CD4 T cell pool while simultaneously differentiating into T_H1 cells in TDLNs and tumours (Fig. 3i,j and Extended Data Fig. 6a,b). By contrast, SMARTA T_{reg} cells primarily retained their FOXP3$^+$ phenotype in both conditions across all tissues examined (Fig. 3i,j and Extended Data Fig. 6a,b). Together, these data show that stem-like CD4 T cells can give rise to T_H1 cells in the cancer environment, but T_{reg} cells actively suppress their differentiation. T_{reg} suppression of stem-like CD4 T cell differentiation also has therapeutic relevance. Despite T_{reg} cells exclusively expressing high levels of CTLA4 in TDLNs and tumours (Extended Data Fig. 6c), only the depleting anti-CTLA4 clone 9H10 (refs. 14,27,28), significantly induced a T_H1 response in both tissues, leading to sustained tumour control in TRAMPC1-GP and orthotopic RENCA kidney cancer models (Extended Data Fig. 6d–j). Together, our findings indicate that tumour-specific stem-like CD4 T cells act as a precursor population to helper or regulatory T cells during the cancer response. Furthermore, these data suggest that differentiation of stem-like CD4 T cells to T_H1 cells might be crucial for effective tumour control and response to immunotherapy.

Requirement of CD4 T cells for CD8 T cell differentiation

Although we found that stem-like CD4 T cells underwent T_H1 differentiation after T_{reg} depletion, it was unclear whether this process contributed to effective anti-tumour immunity. We found that stem-like CD4 T cells were required, given that TRAMPC1-GP and B16F10-GP tumours were not controlled after total CD4 T cell depletion compared with T_{reg} depletion alone (Fig. 4a,b and Extended Data Fig. 7a,b). This CD4-dependent effect was not mediated by direct cytotoxicity, as CD8 T cell depletion in T_{reg}-depleted mice abrogated tumour control in two of the three models examined (Extended Data Fig. 7a–c). These findings highlight the requirement of stem-like CD4 T cells and intact CD8 T cell responses. Therefore, we next examined the effect of T_{reg} cells and stem-like CD4 T cell help on tumour-specific CD8 T cells, using our T_{reg} cell or full CD4 T cell depletion models (Fig. 4a). We found that GP-specific (GP33$^+$) and SPAS1$^+$ (an endogenous tumour antigen) CD8 T cells expanded and underwent robust effector differentiation within

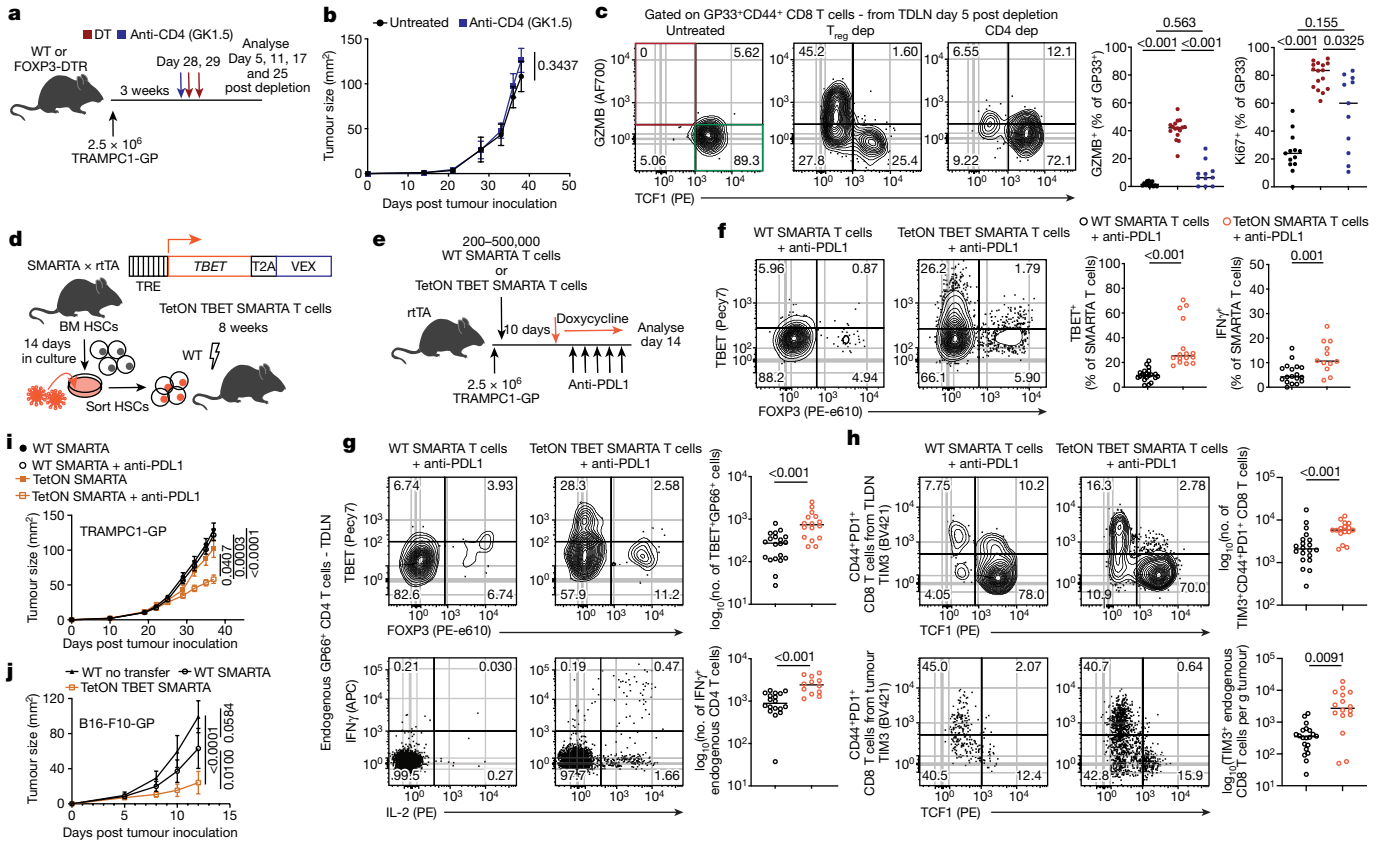

Fig. 4 | Stem-like CD4 to T_H1 differentiation is sufficient to promote effector CD8 T cell responses in TDLNs in the presence of T_{reg} cells. **a**, Experimental design. T_{reg} cells or total CD4 T cells were transiently depleted in TRAMPC1-GP tumour-bearing mice after three to four weeks. **b**, Tumour kinetics as shown by tumour diameter for untreated or total CD4 T cell-depleted mice (untreated, $n = 10$; CD4-depleted, $n = 9$). Data are mean ± s.e.m.; unpaired two-sided Mann–Whitney U test. **c**, Phenotypic analysis of GP33$^+$ CD8 T cells in TDLNs 5 days after T_{reg} or total CD4 T cell depletion ($n = 11$–16 mice per group). Data are median; Kruskal–Wallis test with Dunn's multiple-comparisons tests. **d**, Schematic of construct and process to make TetON TBET SMARTA T cells using a bone marrow (BM) haematopoietic stem cell (HSC) chimera lentiviral system. **e**, Experimental design. **f**, Phenotype and cytokine production of transferred wild-type or TetON TBET SMARTA T cells in TDLNs 14 days after PDL1 therapy in response to GP61–77 peptide stimulation. **g**, Phenotype and cytokine production of endogenous GP66$^+$CD44$^+$ CD4 T cells in TDLNs for each group 14 days after anti-PDL1 therapy in response to GP61–77 peptide stimulation. **h**, Phenotype of bulk activated (CD44$^+$PD1$^+$) CD8 T cells in TDLNs or tumours for each group. **i**, Tumour growth kinetics in TRAMPC1-GP mice for each group. Data are mean ± s.e.m. Data in **f**–**i** represent 3 independent experiments ($n = 4$–6 mice per group for each experiment). Medians are shown in each summary plot; Mann–Whitney U test or Kruskal–Wallis test with Dunn's multiple-comparisons tests where appropriate. **j**, Tumour growth kinetics in B16F10-GP mice that received no SMARTA T cells, wild-type SMARTA T cells or TetON TBET SMARTA T cells. Data are mean ± s.d.; representative of two independent experiments; Kruskal–Wallis test with Dunn's multiple-comparison tests ($n = 5$–7 mice per group for each experiment).

TDLNs five days after T_{reg} depletion (Fig. 4c and Extended Data Fig. 7d,e), a process previously limited to the tumour[29–31]. By contrast, total CD4 T cell depletion resulted in expansion of stem-like CD8 T cells in TDLNs (LN-stem CD8 T cells) with significantly reduced effector differentiation across all models examined (Fig. 4c and Extended Data Fig. 7d–i). In agreement, transcriptional analysis showed that LN-stem CD8 T cells from T_{reg}-depleted mice exhibited unique upregulation of genes related to effector differentiation (*Id2*, *Tbx21*, *Gzmb*, *Ifngr1* and *Cxcr6*) and IFN signalling compared with wild-type and total CD4-depleted mice (Extended Data Fig. 7j–p and Supplementary Table 2). These data suggest a model in which stem-like CD4 T cells or their differentiation into T_H1 cells is required to induce effector output from tumour-specific LN-stem CD8 T cells.

T_H1 cells are sufficient to induce effector CD8 T cells

We next examined whether differentiation of stem-like CD4 T cells to T_H1 cells was sufficient to promote effector CD8 T cell differentiation in TDLNs, even in the presence of T_{reg} cells. Additionally, given the increased expression of cytotoxic molecules on effector CD8 T cells, we also investigated whether promoting differentiation of stem-like CD4 T cells to T_H1 cells could overcome resistance of PDL1 blockade in non-responsive models. To test this, we generated tetracycline-inducible TBET-overexpressing SMARTA T cells (Fig. 4d and Supplementary Data 1c). Upon transfer, these TetON SMARTA T cells expanded and retained a stem-like phenotype in TDLNs prior to doxycycline administration, similar to their wild-type counterparts (Extended Data Fig. 8a). Upon doxycycline administration, TetON SMARTA T cells expressed TBET and produced IFNγ in TDLNs, which was further augmented in response to anti-PDL1 (Fig. 4f and Extended Data Fig. 8a). TetON SMARTA T cell transfer resulted in expansion of endogenous GP66$^+$ and bulk PD1$^+$ stem-like CD4 T cells and T_H1 differentiation with increased IFNγ and IL-2 production in TDLNs and tumours. Notably, this effect was fivefold higher with anti-PDL1 therapy than in untreated and anti-PDL1-treated wild-type SMARTA groups (Fig. 4g and Extended Data Fig. 8b–d). Furthermore, TetON SMARTA T cell transfer in combination with anti-PDL1 resulted in significant expansion and effector differentiation of total PD1$^+$ and GP33$^+$ CD8 T cells in all tissues, leading to tumour control in the unresponsive TRAMPC1-GP model (Fig. 4h,i and Extended Data Fig. 8e–h). TetON

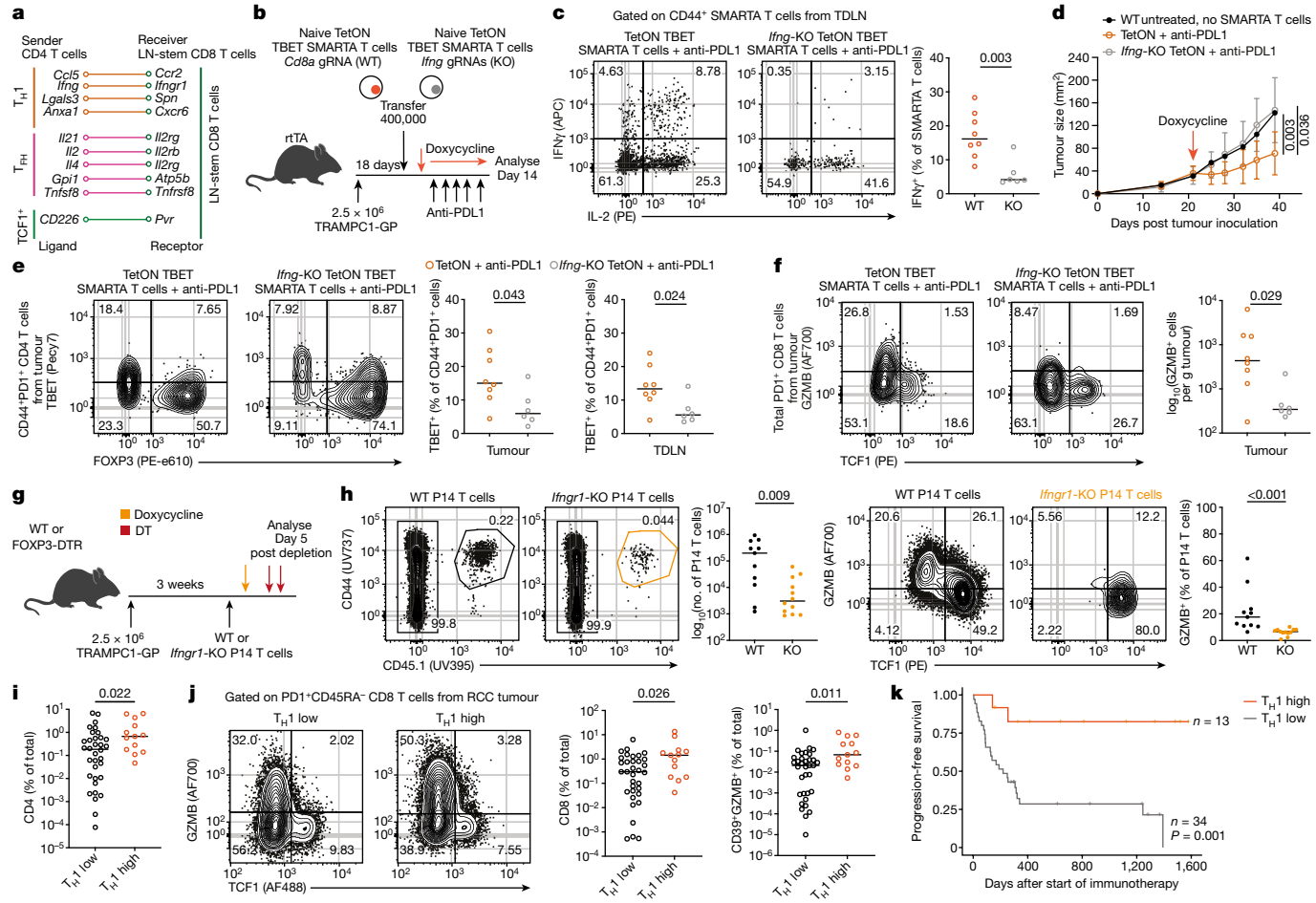

Fig. 5 | T_H1 cell-derived IFNγ is required for differentiation of LN-stem CD8 T cells to effector CD8 T cells in TDLNs. a, NicheNet analysis showing top ligand–receptor interactions between CD4 T cell populations and LN-stem CD8 T cells from T_{reg}-depleted mice. **b**, Experimental design to test the requirement of T_H1 cell-derived IFNγ for effector CD8 T cell differentiation. gRNA, guide RNA. **c**, Cytokine production in response to GP61–77 peptide stimulation for transferred wild-type TetON TBET or *Ifng*-KO TetON TBET SMARTAs in TDLNs 14 days after anti-PDL1 therapy. **d**, Tumour growth kinetics in TRAMPC1-GP mice. Data are mean ± s.d.; Kruskal–Wallis test with Dunn's multiple-comparison tests between groups (untreated, $n = 10$; TetON, $n = 8$; *Ifng*-KO TetON, $n = 6$). **e**,**f**, Phenotype of bulk $PD1^+$ CD4 (**e**) and CD8 (**f**) T cells in tumours 14 days after transfer of TetON or *Ifng*-KO TetON SMARTA T cells with anti-PDL1 therapy. Data are median; two-sided unpaired Mann–Whitney U test ($n = 6$–8 mice per group). **g**, Experimental design to test the intrinsic requirement for IFNγ on tumour-specific stem-like CD8 T cells. **h**, Phenotype of wild-type and inducible *Ifngr1*-KO P14 CD8 T cells in TDLNs five days after T_{reg} depletion. Data are representative of two independent experiments ($n = 5$–6 mice per group for each experiment). Data are median; two-sided unpaired Mann–Whitney U test. **i**,**j**, Total frequency of tumour CD4 T cells and phenotype of tumour $PD1^+CD45RA^-$ CD8 T cells in a cohort of patients with kidney cancer who received immunotherapy. Data are median; two-sided unpaired Mann–Whitney U test. **k**, Disease progression after start of immunotherapy in patients with primary kidney cancer, stratified into those with high or low T_H1 CD4 T cell infiltration in the primary tumour based on optimal cut methods ($n = 47$ patients).

TBET-overexpressing SMARTA T cells also induced robust endogenous $PD1^+$ T_H1 differentiation, resulting in tumour control without the need for checkpoint therapy in B16F10-GP tumours (Fig. 4j and Extended Data Fig. 8i–k). Together, these results indicate that shifting differentiation of stem-like CD4 T cells to T_H1 cells is sufficient to promote effector CD8 T cell differentiation, enhance tumour control and rescue the response to anti-PDL1 therapy, despite the presence of T_{reg} cells.

IFNγ drives CD8 effector T cell differentiation

Given the notable effect of inducing stem-like CD4 to T_H1 differentiation on restoring effector CD8 T cell generation in TDLNs, we next investigated potential mechanisms. NicheNet sender–receiver analysis predicted IFNγ from T_H1 CD4 T cells as a top candidate ligand for induction of transcriptional changes related to effector differentiation on LN-stem CD8 T cells (Fig. 5a and Supplementary Table 3). Indeed, IFNγ receptor (IFNGR1) expression and interferon signalling were upregulated in LN-stem CD8 T cells after T_{reg} depletion, which was not observed in the absence of helper CD4 T cells (Extended Data Fig. 7d–p). Furthermore, we found reduced effector CD8 T cell differentiation in TDLNs accompanied by accelerated tumour growth after T_{reg} depletion when IFNγ, but not IL-12, was systemically blocked in both TRAMPC1-GP and B16F10-GP tumour-bearing mice (Extended Data Fig. 9a–g).

Given these observations, we next examined whether T_H1 cell-derived IFNγ was required to stimulate effector CD8 T cell differentiation and rescue the response to PDL1 blockade. To test this, we generated *Ifng*-knockout (KO) TetON TBET SMARTAs using a CAS9 electroporation system followed by transfer into mice with established TRAMPC1-GP tumours. Compared to TetON SMARTAs, *Ifng*-KO TetON SMARTAs were unable to control TRAMPC1-GP tumours despite the addition of anti-PDL1 therapy (Fig. 5d and Extended Data Fig. 9h,i). *Ifng*-KO TetON SMARTAs did not induce endogenous $GP66^+$ or bulk $PD1^+$ CD4 T cell differentiation to T_H1 cells in TDLNs and tumours (Fig. 5e and Extended Data Fig. 9j), suggesting that IFNγ also has a role in altering the fate of stem-like CD4 T cells. Notably, $GP33^+$ and bulk $PD1^+$ CD8 T cells showed a trend for reduced effector differentiation in TDLNs and significantly

reduced effector CD8 T cell accumulation in the tumour (Fig. 5f and Extended Data Fig. 9k–l). Together, these findings suggest that T_H1 cell-derived IFNγ is involved in promoting stem to effector CD4 and CD8 T cell differentiation, which mediates tumour control and response to anti-PDL1 therapy.

Finally, to examine whether direct IFNγ signalling on stem-like CD8 T cells caused effector differentiation, we generated inducible *Ifngr1*-KO CD8 T cells from P14 mice (Extended Data Fig. 10a and Supplementary Data 1c). Wild-type and *Ifngr1*-KO P14 CD8 T cells were left for three days to similarly activate within TRAMPC1-GP TDLNs and establish a stem cell pool (Extended Data Fig. 10b–d). After three days, mice were treated with doxycycline to knock out *Ifngr1* followed by T_{reg} depletion (Fig. 5g). Five days after T_{reg} depletion, wild-type P14 CD8 T cells underwent robust effector differentiation and upregulated IFNGR1, GZMB and TIM3, with the accompanying loss of TCF1. By contrast, *Ifngr1*-KO P14 CD8 T cells underwent a significantly smaller expansion and retained a stem phenotype in TDLNs (Fig. 5h and Extended Data Fig. 10e–h). Endogenous GP33$^+$ CD8 T cells within the same environment as *Ifngr1*-KO P14 CD8 T cells underwent expansion and effector differentiation in TDLNs (Extended Data Fig. 10i,j), highlighting the direct requirement for IFNγ on LN-stem CD8 T cells. Together, these data suggest a model in which stem-like CD4-to-T_H1 differentiation is sufficient to promote tumour-specific effector CD8 T cell responses in TDLNs. Mechanistically, T_H1 cell-derived IFNγ is intrinsically required by LN-stem CD8 T cells to generate cytotoxic effector cells that mediate tumour control and improve response to anti-PDL1 therapy. Thus, stem-like CD4 T cell fate acts as a switch that regulates restricted or active LN-stem CD8 T cell differentiation states.

T_H1 differentiation predicts immunotherapy response

The data from mouse models predict that patients with cancer who have a robust T_H1 response would have a greater number of cytotoxic effector CD8 T cells and be more responsive to PD1 blockade. Although the majority of activated CD4 T cells within tumours had a TCF1$^+$lin$^-$ phenotype (Fig. 1), around 15% of patients had a significant TBET$^+$ T_H1 CD4 T cell population (Extended Data Fig. 10k). In a cohort of 47 patients with kidney cancer who were receiving immunotherapy, those with robust T_H1 responses in their resected primary tumours had a greater frequency of total and effector GZMB$^+$ CD8 T cells, with significantly better progression-free survival after immunotherapy (Fig. 5i–k and Supplementary Table 5). Of note, patients with T_H1 responses did not exhibit reduced total T_{reg} or stem-like CD4 T cell infiltration within tumours (Extended Data Fig. 10k,l). Additionally, T_H1 CD4 T cell frequency in non-metastatic TDLNs also correlated with effector GZMB$^+$ CD8 T cell frequency in patients with kidney cancer (Extended Data Fig. 10m). Together, these data indicate that human T_H1 CD4 T cell differentiation correlated with a greater number of effector CD8 T cells and improved checkpoint therapy response in patients with kidney cancer. This occurs in the presence of T_{reg} cells, supporting the model that generation of T_H1 cells from stem-like CD4 T cells can induce productive effector CD8 T cell responses.

Discussion

Here we identified a tumour-specific PD1$^+$TCF1$^+$ lineage-negative CD4 T cell with stem-like properties across cancer models and human disease. Found primarily within TDLNs, these cells retained extensive proliferation and differentiation capacity, and shared phenotypic, transcriptional and functional similarities with stem-like CD8 T cells[17,24,29,30,32–34] and precursor CD4 T cells[26,35–38], highlighting parallels in CD4 T cell differentiation between cancer and other chronic diseases. We showed that tumour-specific CD8 T cells are not inherently dysfunctional but can effectively generate effector cytotoxic cells when appropriate CD4 T cell help is provided. Based on our data, we propose two possible fate choices of stem-like CD4 T cells that dictate the outcome of the cancer response (Extended Data Fig. 10n). Early after tumour inoculation, CD4 T cell differentiation is rapidly dominated by T_{reg} cells that through unknown mechanisms restrict tumour-specific CD4 T cells to stem-like or iT_{reg} states. In this restricted fate, stem-like CD4 T cells provide limited help, and antigen-specific CD8 T cell effector differentiation is constrained to the tumour[29–31]. Alternatively, when T_{reg} cells are depleted, stem-like CD4 T cells generate a robust T_H1 response and promote differentiation of LN-stem CD8 T cells to effector CD8 T cells through IFNγ, a model that we defined as active (Extended Data Fig. 10n). Of note, we showed that even in the presence of T_{reg} cells, endogenous stem-like CD4 T cells can generate T_H1 cells, and that this switch in differentiation fate is sufficient to promote effector output from LN-stem CD8 T cells and rescue response to immunotherapy. Finally, we found that human patients with kidney cancer with a robust T_H1 population have a higher frequency of effector CD8 T cells and are highly responsive to immunotherapy. Together, these data highlight that stem-like CD4 T cell fate controls the anti-tumour response by regulating the switch between restricted and active T cell states. Given these observations, we speculate that targeting the large pool of PD1$^+$ stem-like CD4 T cells and promoting their differentiation to T_H1 cells will have important therapeutic implications for enhancing anti-tumour immunity.

Online content

Any methods, additional references, Nature Portfolio reporting summaries, source data, extended data, supplementary information, acknowledgements, peer review information; details of author contributions and competing interests; and statements of data and code availability are available at https://doi.org/10.1038/s41586-024-08076-7.

1. Galon, J. et al. Type, density, and location of immune cells within human colorectal tumors predict clinical outcome. *Science* **313**, 1960–1964 (2006).
2. Herbst, R. S. et al. Predictive correlates of response to the anti-PD-L1 antibody MPDL3280A in cancer patients. *Nature* **515**, 563–567 (2014).
3. Schreiber, R. D., Old, L. J. & Smyth, M. J. Cancer immunoediting: integrating immunity's roles in cancer suppression and promotion. *Science* **331**, 1565–1570 (2011).
4. Borst, J. et al. CD4$^+$ T cell help in cancer immunology and immunotherapy. *Nat. Rev. Immunol.* **18**, 635–647 (2018).
5. Speiser, D. E. et al. CD4$^+$ T cells in cancer. *Nat. Cancer* **4**, 317–329 (2023).
6. Cohen, M. et al. The interaction of CD4$^+$ helper T cells with dendritic cells shapes the tumor microenvironment and immune checkpoint blockade response. *Nat. Cancer* **3**, 303–317 (2022).
7. Magen, A. et al. Intratumoral dendritic cell–CD4$^+$ T helper cell niches enable CD8$^+$ T cell differentiation following PD-1 blockade in hepatocellular carcinoma. *Nat. Med.* **29**, 1389–1399 (2023).
8. Cui, C. et al. Neoantigen-driven B cell and CD4 T follicular helper cell collaboration promotes anti-tumor CD8 T cell responses. *Cell* **184**, 6101–6118.e13 (2021).
9. Sharma, P. et al. Immune checkpoint therapy—current perspectives and future directions. *Cell* **186**, 1652–1669 (2023).
10. Binnewies, M. et al. Unleashing type-2 dendritic cells to drive protective antitumor CD4$^+$ T cell immunity. *Cell* **177**, 556–571.e16 (2019).
11. Kim, J. M., Rasmussen, J. P. & Rudensky, A. Y. Regulatory T cells prevent catastrophic autoimmunity throughout the lifespan of mice. *Nat. Immunol.* **8**, 191–197 (2007).
12. Lahl, K. et al. Selective depletion of Foxp3$^+$ regulatory T cells induces a scurfy-like disease. *J. Exp. Med.* **204**, 57–63 (2007).
13. Spitzer, M. H. et al. Systemic immunity is required for effective cancer immunotherapy. *Cell* **168**, 487–502.e15 (2017).
14. Wei, S. C. et al. Distinct cellular mechanisms underlie anti-CTLA-4 and anti-PD-1 checkpoint blockade. *Cell* **170**, 1120–1133.e17 (2017).
15. Alonso, R. et al. Induction of anergic or regulatory tumor-specific CD4$^+$ T cells in the tumor-draining lymph node. *Nat. Commun.* **9**, 2113 (2018).
16. Nishikawa, H. & Sakaguchi, S. Regulatory T cells in tumor immunity. *Int. J. Cancer* **127**, 759–767 (2010).
17. Jansen, C. S. et al. An intra-tumoral niche maintains and differentiates stem-like CD8 T cells. *Nature* **576**, 465–470 (2019).
18. Zhou, L., Chong, M. M. & Littman, D. R. Plasticity of CD4$^+$ T cell lineage differentiation. *Immunity* **30**, 646–655 (2009).
19. Zhu, J., Yamane, H. & Paul, W. E. Differentiation of erffector CD4 T cell populations. *Annu. Rev. Immunol.* **28**, 445–489 (2010).
20. Brummelman, J. et al. High-dimensional single cell analysis identifies stem-like cytotoxic CD8$^+$ T cells infiltrating human tumors. *J. Exp. Med.* **215**, 2520–2535 (2018).
21. Hong, S.-W. et al. Immune tolerance of food is mediated by layers of CD4$^+$ T cell dysfunction. *Nature* **607**, 762–768 (2022).
22. Kalekar, L. A. et al. CD4$^+$ T cell anergy prevents autoimmunity and generates regulatory T cell precursors. *Nat. Immunol.* **17**, 304–314 (2016).

23. Barber, D. L. et al. Restoring function in exhausted CD8 T cells during chronic viral infection. *Nature* **439**, 682–687 (2006).
24. Im, S. J. et al. Defining CD8$^+$ T cells that provide the proliferative burst after PD-1 therapy. *Nature* **537**, 417–421 (2016).
25. Siddiqui, I. et al. Intratumoral Tcf1$^+$ PD-1$^+$ CD8$^+$ T cells with stem-like properties promote tumor control in response to vaccination and checkpoint blockade immunotherapy. *Immunity* **50**, 195–211.e10 (2019).
26. Xia, Y. et al. BCL6-dependent TCF-1+ progenitor cells maintain effector and helper CD4$^+$ T cell responses to persistent antigen. *Immunity* **55**, 1200–1215.e6 (2022).
27. Du, X. et al. A reappraisal of CTLA-4 checkpoint blockade in cancer immunotherapy. *Cell Res.* **28**, 416–432 (2018).
28. Simpson, T. R. et al. Fc-dependent depletion of tumor-infiltrating regulatory T cells co-defines the efficacy of anti–CTLA-4 therapy against melanoma. *J. Exp. Med.* **210**, 1695–1710 (2013).
29. Prokhnevska, N. et al. CD8$^+$ T cell activation in cancer comprises an initial activation phase in lymph nodes followed by effector differentiation within the tumor. *Immunity* **56**, 107–124.e5 (2023).
30. Connolly, K. A. et al. A reservoir of stem-like CD8$^+$ T cells in the tumor-draining lymph node preserves the ongoing antitumor immune response. *Sci. Immunol.* **6**, eabg7836 (2021).
31. Li, Z. et al. In vivo labeling reveals continuous trafficking of TCF-1$^+$ T cells between tumor and lymphoid tissue. *J. Exp. Med.* **219**, e20210749 (2022).
32. Alfei, F. et al. TOX reinforces the phenotype and longevity of exhausted T cells in chronic viral infection. *Nature* **571**, 265–269 (2019).
33. Gearty, S. V. et al. An autoimmune stem-like CD8 T cell population drives type 1 diabetes. *Nature* **602**, 156–161 (2022).
34. Eberhardt, C. S. et al. Functional HPV-specific PD-1$^+$ stem-like CD8 T cells in head and neck cancer. *Nature* **597**, 279–284 (2021).
35. Moguche, A. O. et al. ICOS and Bcl6-dependent pathways maintain a CD4 T cell population with memory-like properties during tuberculosis. *J. Exp. Med.* **212**, 715–728 (2015).
36. Shin, B. et al. Effector CD4 T cells with progenitor potential mediate chronic intestinal inflammation. *J. Exp. Med.* **215**, 1803–1812 (2018).
37. Zou, D. et al. CD4$^+$ T cell immunity is dependent on an intrinsic stem-like program. *Nat. Immunol.* **25**, 66–76 (2024).
38. Kratchmarov, R. et al. TCF1–LEF1 co-expression identifies a multipotent progenitor cell (T_H2-MPP) across human allergic diseases. *Nat. Immunol.* **25**, 902–915 (2024).

Methods

Human sample processing and flow cytometry

Patients were recruited in accordance with Emory University Institutional Review Board protocol (IRB00055316), with all patients providing informed consent. Tumours and TDLNs were collected from patients undergoing partial or radical nephrectomy, prostatectomy, or transurethral surgery for resection of kidney, prostate or bladder tumours. No statistical methods were used to predetermine sample size. Samples were maintained in Hank's Balanced Salt solution until processing. Samples were then cut into small pieces, digested with a collagenase/liberase enzyme cocktail, and homogenized using a MACS dissociator. Digested tumours were then washed with buffer through a 70-μm filter into a single-cell suspension. Samples were then lysed using red blood cell ACK lysis buffer or ice-cold water followed by an equal volume of 1.8% of NaCl solution, followed by a 44% Percoll/RPMI gradient. Single-cell suspensions were then either used fresh or frozen in freezing medium (FBS + 10%DMSO) at −80 °C for future use.

For flow cytometry, single-cell suspensions were stained with antibodies listed in Supplementary Table 1 for 30 min at 4 °C or on ice in fluorescence-activated cell sorting (FACS) buffer. Fixable near-IR or aqua dead cell staining kit (Invitrogen) was used for live/dead staining. For intracellular staining, cells were permeabilized using the FOXP3 Fixation/Permeabilization kit (eBioscience) in fixation buffer for 45 min at 4 °C. Cells were then stained for transcription factors and intracellular molecules in permeabilization buffer for 30 min at 4 °C or on ice. After washing, samples were acquired in a Symphony instrument (BD Biosciences) and analysed using FlowJo (v10).

Human in vitro stimulations, co-cultures and functional analyses

Single-cell suspensions from fresh or frozen human tumour samples were stained with CTV according to manufactures instructions (Thermo) at a concentration of 1 μl CTV per 10 million cells in PBS. If frozen samples were used for stimulation, cells were rested in 10% supplemented RPMI at 37 °C for 4 h prior to sort. CTV-labelled stem-like and $CD39^+$ T_{reg} cells/$EOMES^+$ CD4 T cells were sorted according to the gating strategy in Supplementary Data 1a in the Becton Dickinson FACS Aria II Cell Sorter. Stem-like CD4 T cells were defined as live $CD4^+PD1^+CD45RA^-CD28^+CD26^+CD127^+CD39^-$, $CD39^+$ effectors were defined as live $CD4^+PD1^+CD45RA^-CD28^+CD26^-CD127^-CD39^+$ (representative plots for sorting strategy shown in Supplementary Data 1a). For differentiating between T_{reg} cells and EOMES CD4 T cells, CD25 and CD38 were used to distinguish these two populations. Sorted CD4 populations were cultured in 96-well U bottom plates in supplemented T cell medium (RPMI, 10% FBS, 1% penicillin-streptomycin, 1% L-glutamine, 1% sodium pyruvate, 1% non-essential amino acids, 0.0005% 2-mercaptoethanol) and 10–20 U ml^{-1} IL-2 (Peprotech). Stimulating conditions were performed using anti-CD3/CD28/CD2 beads (Miltenyi Biotech) at a ratio of 1 bead for 2 CD4 T cells and polarization cytokines according to the condition. T_H0 condition: 10–20 U ml^{-1} IL-2, T_H1 condition: 10–20 U ml^{-1} IL-2, 10 ng ml^{-1} IL-12; T_{reg} condition: 10–20 U ml^{-1} IL-2, 10 ng ml^{-1} TGFβ, 1 μg ml^{-1} anti-IFNγ; EOMES condition: 10–20 U ml^{-1} IL-2, 10 ng ml^{-1} IL-12, 50 ng ml^{-1} IL-4, 1 μg ml^{-1} anti-IFNγ; T_{FH} condition: 50 ng ml^{-1} activin A, 5 ng ml^{-1} IL-12. Samples were analysed 5 days after stimulation by flow cytometry for proliferation as well as expression of transcription factors and various molecules.

For dendritic cell co-cultures, CTV-labelled $PD1^+$ stem-like, $CD39^+$ CD4 T cells and bulk dendritic cells ($CD3^-HLA\text{-}DR^+CD11c^+$) were sorted from matched patient tumours as shown in Supplementary Data 1a. Sorted dendritic cells were irradiated with 10 Gy prior to being placed in culture. Co-cultures were plated at one dendritic cell per one CD4 T cell population for as many cells as possible based on the number of cells recovered for each patient. Samples were analysed five days after stimulation by flow cytometry for proliferation as well as expression of transcription factors and various molecules. For experiments where exogenous IL-12 was provided, 10 ng ml^{-1} IL-12 was added to the dendritic cell–CD4 T cell well at the time of plating.

For high-dose stimulation assays, 4,000 U ml^{-1} IL-2 was used in combination with CD3/CD28/CD2 beads at a ratio of 1 bead for 2 CD4 T cells. $CD39^+$ CD4 T cells were analysed five days after stimulation by flow cytometry.

To calculate the frequency of original cells that underwent division, we used the following calculation: X = (sum of percentage of cells in division $i/2^i$), where i = 1:5. To obtain the final percentage of original cells we used the formula $X/(X + Y)$, where Y is the percentage of undivided cells.

Mice

Animal experiments were conducted and designed in accordance with National Institutes of Health and the Emory University Institutional Animal Care and Use Committee guidelines and approved under PROTO201800261. Mice were housed in a 07:00–19:00 light cycle, 22 °C and controlled 40–50% humidity in clean pathogen-free rooms. C57BL/6 J mice (000664) and Pep Boy mice (B6.SJL-$Ptprc^a$ $Pepc^b$/BoyJ, 002014) were purchased from Jackson laboratories between the ages of 7–10 weeks. LCMV DbGP33-specific TCR transgenic P14 mice were a gift from the laboratory of R. Ahmed and were bred and maintained at Emory University. LCMV GP66-77-specific SMARTA mice (030450) were purchased from Jackson laboratories and were bred and maintained at Emory University. FOXP3-DTR mice (DEREG, 032050-JAX) expressing the human diphtheria toxin receptor and the GFP reporter[12] were purchased from Jackson laboratories and used for T_{reg} depletion experiments. rtTA (Rosa26-CAGs-rtTA3 knock-in, 029627) mice were purchased from Jackson laboratories, bred in house and crossed with transgenic SMARTA mice for TBET overexpression experiments. iCas9 (B6;129S4-Gt(ROSA)26Sortm1(rtTA*M2)Jae Col1a1tm1(tetO-cas9)Sho/J, 029415) mice were purchased from Jackson laboratories, bred in house and crossed with rtTA mice for inducible knockout experiments. For tumour experiments, male C57BL/6J mice were used for the TRAMPC1-GP cell line, while female and male C57BL/6J mice were used for B16F10-GP and MC38 experiments. Female Balb/c mice were used for RENCA-HA or orthotopic RENCA-HA-luciferase experiments.

Tumour cell lines, subcutaneous injection and orthotopic surgical renal implants

Tumours were scored according to Emory University tumour burden policy 303, where any individual tumour >20 mm in any diameter was considered endpoint, as indicated by PROTO201800261. Mice were randomized to experimental groups to normalize for tumour sizes prior to the start of treatments. No statistical methods were used to predetermine sample size. Investigators were not blinded to group allocation during experimental setup, data collection, or analysis. TRAMPC1 cell line was obtained from American Type Culture Collection (ATCC) and full length LCMV glycoprotein was added using lentiviral transduction[29]. B16 F10 was obtained from ATCC and the full length LCMV glycoprotein was made by lentiviral transduction in the laboratory of R. Ahmed. B16F10-GP cell line was a gift from the laboratory of R. Ahmed. The MC38 cell line was obtained from ATCC. The RENCA cell line was obtained from ATCC and transduced using a lentivirus containing the influenza haemagglutinin (HA) for stable RENCA-HA transduction. RENCA-HA-luciferase was made in house by an additional transduction of a lentiviral plasmid containing luciferase and neomycin. Cells were selected on neomycin resistance for 10 days. All cells were cultured at 37 °C in 5% CO_2 in appropriate media. All cell lines were tested annually for mycoplasma infection and tested negative. For tumour inoculation, cells were detached from culture using 0.05% trypsin and saturated with respective media. Cells were then washed with PBS twice and resuspended in PBS at different concentrations and every mouse was injected with 100 μl subcutaneously at the following

concentrations: TRAMPC1-GP 2.5×10^6 cells, B16F10-GP 2.5×10^5 or 5×10^5 cells, MC38 2.5×10^5 cells, and RENCA-HA 2.5×10^5 cells.

RENCA-HA-luciferase cells were prepared as described above. Prior to surgical implant, RENCA-HA-luciferase cells were mixed at a 1:1 ratio with Matrigel (356231 Corning) for a final 1×10^5 cell concentration per mouse in 20 µl. For orthotopic RENCA-HA-luciferase tumour experiments, Balb/c female mice were placed under isoflurane anaesthetic and received 0.5 mg kg^{-1} bupenorphrine SR (sustained release) and 6 mg kg^{-1} of lidocaine subcutaneously. Mice were shaved along the right flanks and skin was disinfected with Prevantics swabs. A small vertical incision was made on the right lateral side of the mouse above the kidney. The kidney was then lifted upon the body surface and the mixture of cells and Matrigel was injected using a low-dose insulin syringe into the subcapsular space of the kidney. 6-O absorbable sutures were used for musculature closure and 5-O non-absorbable synthetic sutures were used to close the skin. After 7 days, Balb/c mice were injected with 200 µl D-luciferin potassium salt/PBS solution into the intraperitoneal space for 8 min for in vivo bioluminescence imaging to confirm tumour growth prior to the start of treatment.

TRAMPC1-GP cells were cultured in DMEM with glucose supplemented with 10% FBS (Corning), 1% L-glutamine, 1% penicillin-streptomycin, dehydroisoandrosterone (1.65 µg), and insulin (2.5 mg). B16F10-GP cells were cultured in DMEM with glucose supplemented with 10% FBS (Corning), 1% L-glutamine, 1% penicillin-streptomycin and 1% sodium pyruvate. MC38 cells were cultured in DMEM with glucose supplemented with 10% FBS (Corning), 1% L-glutamine, 1% penicillin-streptomycin, 1% sodium pyruvate and 1% 100× non-essential amino acids and 10 mM HEPES. RENCA-HA and RENCA-HA-luciferase cells were cultured in RPMI with 10% FBS (Corning), 1% L-glutamine, 1% penicillin-streptomycin, 1% sodium pyruvate and 1% 100× non-essential amino acids. All cell lines used were negative for Mycoplasma and other infectious agents.

Mouse tissue processing and flow cytometry staining

Tumours, lymph nodes, spleens and lungs were collected and digested in collagenase D (2 mg ml^{-1}) shaking for 25 min at 37 °C. Inguinal, axillary and brachial lymph nodes on the side of tumour inoculation were pooled as TDLNs. All digested tissues were washed with RPMI supplemented with 2–5%FBS through a 70-µm filter into single-cell suspension. Tumours and spleen were RBC lysed using ACK lysis solution and resuspended in 2–5% RPMI. Tumours went through an additional 44% Percoll/RPMI gradient for 10 min to remove excess fat prior to staining. Livers and lungs went through a 44% and 67% Percoll gradient for 20 min to remove excess fat and hepatocytes. Mouse tissues were stained with antibodies listed in Supplementary Table 1. For extracellular staining, cells were stained for 30 min at 4 °C on ice in FACS buffer. Cells were then washed and fixed in FOXP3 Fixation/Permeabilization kit (eBioscience) for 25 min at room temperature or overnight at 4 °C. For intracellular staining, cells were stained in permeabilization buffer for 30–45 min at room temperature if fixation was performed at room temperature or on ice if cells were fixed overnight. For intracellular cytokine staining, total cells from TDLNs were cultures in RPMI supplemented with 10% FBS in the presence of 2 µg ml^{-1} of LCMV GP61–80 peptide (GLKGPDIY KGVYQFKSVEFD), 1 µg ml^{-1} of Brefeldin A (BD) and 2 µg ml^{-1} of Monesin (BD) for 5 h at 37 °C before staining. Cells for intracellular staining were staining for live/dead and surface proteins. Fixation was performed using the BD Cytofix/Cytoperm kit according to the manufacturer's instructions. After 20 min at 4 °C, IFNγ, TNF and IL-2 (BD) were stained in BD permeabilization buffer for 30 min on ice. Data was acquired on a Beckton Dickinson LSRII or a Symphony instrument (BD Biosciences). All CD4 and CD8 tetramers were acquired from the NIH tetramer core facility at Emory University, supported by contract 75N93020D0000.

Adoptive transfers and LCMV Armstrong infection

For adoptive transfers, spleens from congenically mismatched GP33-transgenic P14 mice, GP61–77 transgenic SMARTA mice, or any of the crosses iCAS9 × P14 rtTA SMARTA mice were collected. Splenocytes were processed in sterile conditions as described above. No collagenase digestion was performed for adoptive transfers. CD8 and CD4 T cells were isolated using EasySep mouse CD8 isolation (19853) or naive CD4 negative selection (19765) kits (StemCell), respectively. For tumour experiments, 250,000 to 1 million isolated P14 CD8 T cells and 200,000–500,000 naive SMARTA CD4 T cells were transferred intravenously unless otherwise specified for an experiment. For LCMV Armstrong infection experiments, 1,000–5,000 P14 CD8 T cells were transferred intravenously.

For TDLN SMARTA re-transfer experiments, activated stem-like SMARTA CD4 T cells were sorted according to Supplementary Data 1b and 400–3,000 sorted cells were transferred intravenously into naive mice that were subsequently infected with LCMV Armstrong. Mice were infected with 2×10^5 pfu of LCMV Armstrong via intraperitoneal injection as previously described[39].

For TDLN re-transfer experiments into tumour-matched mice, $CD45.1^+PD1^+$ stem-like or T_{reg} SMARTA cells were sorted according to Supplementary Data 1d. A total of 5,000–20,000 cells was transferred intravenously via tail vein into 2- to 3-week-old TRAMPC1-GP tumour-bearing $CD45.2^+$ WT or FOXP3-DTR mice. SMARTAs were left untreated for 2 days followed by 1 µg of diphtheria toxin administration. Mice were analysed 5 days after diphtheria toxin administration and 7 days after transfer.

In vivo treatments and depletions

T_{reg} cells were depleted in FOXP3-DTR (DEREG) mice bearing tumours by intraperitoneal injection of 1 µg of diptheria toxin (Sigma) diluted in endotoxin-free PBS on two consecutive days. CD4 T cells were depleted by intraperitoneal injection of 300 µg anti-CD4 antibody (GK1.5) diluted in endotoxin-free PBS. For cytokine blocking experiments, anti-IL-12p40 (250 µg, BioXcell) or anti-IFNγ (250 µg, BioXcell) antibodies were injected intraperitoneally every other day for the duration of the experiment. CD8 T cells were depleted with 250 µg per mouse of anti-CD8b (Lyt 3.2) antibody intraperitoneally every other day. For PDL1 or CTLA4 blocking experiments, 200 µg of anti-PDL1 (10 F.9G2, BioXcell), anti-CTLA4 (4F10, BioXcell) or anti-CTLA4 (9H10, BioXcell) were administered intraperitoneally every three days. Doxycycline hyclate (Sigma) was administered with one dose (25 mg kg^{-1}) of intraperitoneal injection followed by administration in drinking water at a concentration of 2 mg ml^{-1} supplemented with 2% sucrose in sterile conditions to induce CAS9 or to overexpress TBET.

10x scRNA-seq and analysis

For human scRNA-seq, tumour single-cell suspensions were stained and sorted on a Beckton Dickinson FACS Aria II Cell Sorter. Activated CD4 T cells were sorted based on live $CD3^+CD4^+CD8^-PD1^+CD45RA^-$ from kidney tumours from two separate patients. For mouse scRNA-seq, activated CD4 T cells were sorted based on live $CD4^+CD8^-PD1^+CD44^+CD19^-B220^-HLADR-$, activated CD8 T cells were sorted based on live $CD4^-CD8^+PD1^+CD44^+CD19^-B220^-HLADR^-$ from TDLNs of wild-type ($n = 12$ pooled mice), T_{reg}-depleted ($n = 4$ pooled mice) and CD4-depleted ($n = 4$ pooled mice) mice. Naive CD4 and CD8 T cells ($PD1^-CD44^-CD62L^+$) were spiked into each respective sample. scRNA-seq libraries were made using the Chromium single-cell 5′ Library and Gel Bead kit (10x Genomics). Sorted cells were sorted and captured into the Gel Beads-in-emulsion (GEMs). After the reverse transcription GEMs were disrupted and cDNA was isolated and pooled. The barcoded cDNA was fragmented, end repaired, and A-tails were added followed by sample index PCR. The purified libraries were sequenced to 50,000 reads per cell on a HiSeq300 (Illumina) with 26 cycles for 1,8 cycles for index (i7) and 91 cycles for read 2.

For data processing, samples were aligned, filtered and counted for barcodes and unique molecular identifiers using Cellranger v3.1. Data were further analysed using R v4.1.2 and the Seurat package v4.0.3

(ref. 40). For human scRNA-seq, cells with a percentage of mitochondrial genes below 7% were included. Cells with more than 3,000 or fewer than 200 genes were considered outliers and were excluded from downstream analysis. For the mouse scRNA-seq, cells with a percentage of mitochondrial genes below 7% were included. Cells with more than 4,000 or fewer than 500 genes were considered outliers and were excluded from downstream analysis. Samples from different groups or different patients were merged using the FindIntegrationMarkers function in the Seurat package. Principal components analysis was performed, and the top eight to ten most significant components were used for clustering. Differentially expressed genes within each cluster or treatment were identified by the Seurat function FindAllMarkers for volcano plots. Differentially expressed genes between CD8 T cell and CD4 T clusters are provided in Supplementary Table 2. Gene set enrichment analysis was performed using the VISION R package v.3.0 (ref. 41) using the signatures in Supplementary Table 4 for human CD8 T cell stem-like signature, T_{reg} signature, T_H1 signature, cell cycle signature, human T_{FH} signature, mouse IFNγ signalling signature and mouse CD4 precursor TCF1$^+$ signature[26]. Signatures of human CD4 stem-like, EOMES$^+$ and T_{reg} tumour-infiltrating lymphocytes from our study from differentially expressed genes on our scRNA-seq are included in Supplementary Table 4. For TCR analysis, TCR clonotypes were aligned using CellRanger v3.1 and V, D, J gene segments were aligned using MixCR v3.0 (ref. 42). TCRα chains were filtered and unique clonotypes between populations were defined by matching CDR3 beta sequences.

NicheNet analysis

NicheNet ligand–receptor analysis was performed between TDLN CD4 and CD8 T cell populations in wild-type and T_{reg}-depleted mice. In brief, separate Seurat objects containing CD4 T cells and CD8 T cells were included to contain cells derived from each treatment group: untreated, T_{reg} depletion and total CD4 T cell depletion. We set the different helper CD4 T cells (clusters 1–4) as sender populations and stem-like CD8 T cells as the receiver population for each group. For target ligands, we performed differentially expressed gene analysis (average log fold change > 0.25 and $P < 0.05$) between wild-type and T_{reg}-depleted CD4 T cell subsets and chose the top significant ligands within each CD4 T cell population. For the receiver stem-like CD8 T cell population, we focused our analysis on the most differentially expressed receptors (average log fold change > 0.25 and $P < 0.05$) between T_{reg}-depleted mice when compared to wild-type and CD4-depleted mice that were associated with effector differentiation and analysed the top ten ligand–receptor pairs. Scoring of the predicted ligand–receptor pairs based on the NicheNet vignette Pearson correlation analysis[43]. NicheNet scores are provided in Supplementary Table 3.

HSC expansion and bone marrow chimeras

Chimeras for knockout and overexpression functional experiments were made using a haematopoietic stem cell bone marrow system (Supplementary Data 1c). Femurs, tibias and hips were isolated from donor mice. Bones were cleaned and bone marrow was extracted by flushing the bones with a syringe and RPMI with 2% FBS. Red blood cells in the cell suspension were then lysed using ACK lysis buffer and cells were surface stained in FACS buffer for 30 min with antibodies listed in Supplementary Table 1. Lin$^-$SCA1$^+$cKIT$^+$ (LSK) cells were sorted and plated in fibronectin coated plates (R&D and Corning). Sorted donor HSCs were expanded for 2- to 3-weeks in albumin-free culture F12 medium supplemented with 1% Insulin-Transferrin-Selenium-Ethanolamine (Thermo), 1% penicillin-streptomycin-gentamycin (Thermo), 10 mM HEPES (Thermo), 100 ng ml^{-1} mouse thrombopoietin (Pepro, Fugifilm), 10 ng ml^{-1} mouse SCF (Pepro), and 0.1% polyvinyl alcohol as previously described[44]. Donor bone marrow HSCs varied according to the experiment from the following mice: iCAS9 × P14 or rtTA × SMARTA.

Expanded HSCs were then spinfected in retronectin (20 μg ml^{-1})/fibronectin coated plates at 1,700*g* for 90 min at 32 °C with a lentivirus carrying the single guide RNA (sgRNA) of interest with the fluorescent reporter VEX to mark infected cells. For TBET overexpression experiments, expanded HSCs were infected with a lentivirus carrying a tetracycline promoter and a shortened N-terminus TBET sequence, producing a protein of 513 amino acids, that was attached to T2A and the VEX reporter. Transgene positive (VEX$^+$) HSCs were then sorted to reconstitute lethally irradiated recipient mice (Supplementary Data 1c). Mice were irradiated with 2 doses of 5.75 Gy 6 h apart. For TBET overexpression experiments, bulk LSK$^+$ cells were sorted to reconstitute irradiated mice, given that VEX expression was under the control of doxycycline. Mice were kept on sterile cages under administration of neomycin antibiotics in their water for 3-weeks after irradiation. Chimerism was assessed 8–10 weeks after transfer by bleeding and experiments were performed between 10 and 14 weeks after reconstitution.

Lentiviral constructs and guide RNA design

The sgRNAs for knockout experiments were designed using the CHOP-CHOP design tool[45]. sgRNAs were cloned into the pXPR_053 vector (Addgene 113591) using a BsmBI restriction digest. sgRNA sequences are listed in Supplementary Table 1 for IFNGR1. For TBET overexpression experiments, we generated the TBET-T2A-VEX construct (Supplementary Data 1d and Supplementary Table 1) and inserted the full sequence into the pTet-IRES-EGFP plasmid (Addgene #64238) using PmeI and SalI cloning sites.

CRISPR–CAS9 gene editing and adoptive transfer

To generate TetON TBET *Ifng*-KO SMARTAs, sgRNAs targeting mouse *Ifng* (5′-GGCTTTCAATGACTGTGCCG-3′, Mm.Cas9.IFNG.1.AA) and (5′-AAGAGATAATCTGGCTCTGC-3′, Mm.Cas9.IFNG.1.AC) were obtained from IDT (Supplementary Table 1). A sgRNA targeting mouse *Cd8a* was used as a control (5′-CGTCCCACGTTATCTTGTTG-3′, Mm.Cas9.CD8A.1.AA). In brief, naive TetON TBET SMARTA T cells were isolated from the spleen of chimeric mice using the EasySep naive CD4 negative selection kit (StemCell). Guides were mixed with a tracrRNA (1075928, IDT) and incubated at 95 °C for 4 min. Guide or *trans*-activating CRISPR RNA (tracrRNA) was left to return to room temperature prior to adding CAS9 Nuclease (1081058, IDT). Naive CD4 T cells were then prepared in the primary cell nucleofector solution (V4XP-3032, Lonza) and mixed with the CAS9–RNP mixture and transferred to the 4D-Nucleofector 96-well shuttle. Cells were electroporated using a mouse unstimulated T cell programme in the 4D-Nucleofector unit. Cells were allowed to rest for 30 min in complete RPMI at 37 °C followed by adoptive transfer via tail vein intravenous injection.

Quantification and statistical analyses

Statistical analysis was performed with Prism (v9.0, GraphPad). Two-tailed unpaired Mann–Whitney U tests, One-way ANOVA with Tukey's multiple-comparison test or Kruskal–Wallis test with Dunn's multiple-comparison tests were used when appropriate and as indicated in each figure legend for human and mouse data. For survival analysis, follow up time was calculated as the number of days from the date of surgery to an event (disease progression or death) or to censorship. Patients who had not progressed or were not deceased were censored, and the number of days is calculated from the date of surgery to 5 January 2023. The T_H1 high and low patient groups were stratified based on the optimal cut-off value. Investigators were not blinded during outcome assessment. Statistical significance was defined as $P < 0.05$ and individual P values are listed for each summary graph.

Reporting summary

Further information on research design is available in the Nature Portfolio Reporting Summary linked to this article.

Data availability

Raw fastq files and associated scRNA sequencing have been uploaded to the NCBI Gene Expression Omnibus (GEO) database under identifier GSE274801. Other relevant data are available from the corresponding author upon reasonable request. Source data are provided with this paper.

39. Matloubian, M., Concepcion, R. J. & Ahmed, R. $CD4^+$ T cells are required to sustain $CD8^+$ cytotoxic T-cell responses during chronic viral infection. *J. Virol.* **68**, 8056–8063 (1994).
40. Hao, Y. et al. Integrated analysis of multimodal single-cell data. *Cell* **184**, 3573–3587.e29 (2021).
41. Jones, M. G., Rosen, Y. & Yosef, N. Interactive, integrated analysis of single-cell transcriptomic and phylogenetic data with PhyloVision. *Cell Rep. Methods* **2**, 100200 (2022).
42. Bolotin, D. A. et al. MiXCR: software for comprehensive adaptive immunity profiling. *Nat. Methods* **12**, 380–381 (2015).
43. Browaeys, R., Saelens, W. & Saeys, Y. NicheNet: modeling intercellular communication by linking ligands to target genes. *Nat. Methods* **17**, 159–162 (2020).
44. Wilkinson, A. C. et al. Long-term ex vivo haematopoietic-stem-cell expansion allows nonconditioned transplantation. *Nature* **571**, 117–121 (2019).
45. Labun, K. et al. CHOPCHOP v3: expanding the CRISPR web toolbox beyond genome editing. *Nucleic Acids Res.* **47**, W171–W174 (2019).

Acknowledgements This work was supported by the James M. Cox Foundation, and J. C. Kennedy, funding from the Prostate Cancer Foundation and pilot funding from the Winship Cancer Institute supported by the Dunwoody Country Club Senior Men's Association; H.T.K. was supported by the Cancer Research Institute Lloyd J. Old STAR program. NCI grants 1R01CA280069 (to H.T.K.) and U01-CA113913 (to M.G.S.); DOD grants W81XWH-20-1-0525 (to H.T.K. and V.A.M.) and HT9425-23-1-0318 (H.T.K.). H.T.K. was supported by ARPA-H funding (1AY1AX000001) C.B.M. was supported by the Howard Hughes Medical Institute Hanna H. Gray Fellowship (GT16001), the Burroughs Wellcome Fund – PDEP Fellowship (1022362) and the Cancer Research Institute Bristol Myers Squibb Fellowship (CRI4061). The authors acknowledge the Yerkes NHP Genomics Core (P51 OD011132, NIH S10 OD026799) and the Emory Flow Cytometry Core (UL1TR002378). All Tetramers were acquired from the NIH tetramer core, supported by contract 75N93020D0000.

Author contributions M.A.C. and H.T.K. designed the study, analysed data and composed the manuscript. M.A.C. conducted experiments with support from N.P., E.S., P.G. and R.M.V. R.G., L.D. and P.G. collected human tissue samples and organized clinical data. M.A.B., S.J., V.N., V.A.M. and M.G.S. provided clinical samples. N.P., E.S., C.B.M. and R.M.V, provided critical expertise and assisted in result interpretation. All authors reviewed the manuscript.

Competing interests The authors declare no competing interests.

Additional information

Supplementary information The online version contains supplementary material available at https://doi.org/10.1038/s41586-024-08076-7.

Correspondence and requests for materials should be addressed to Haydn T. Kissick.

Peer review information *Nature* thanks the anonymous reviewer(s) for their contribution to the peer review of this work.

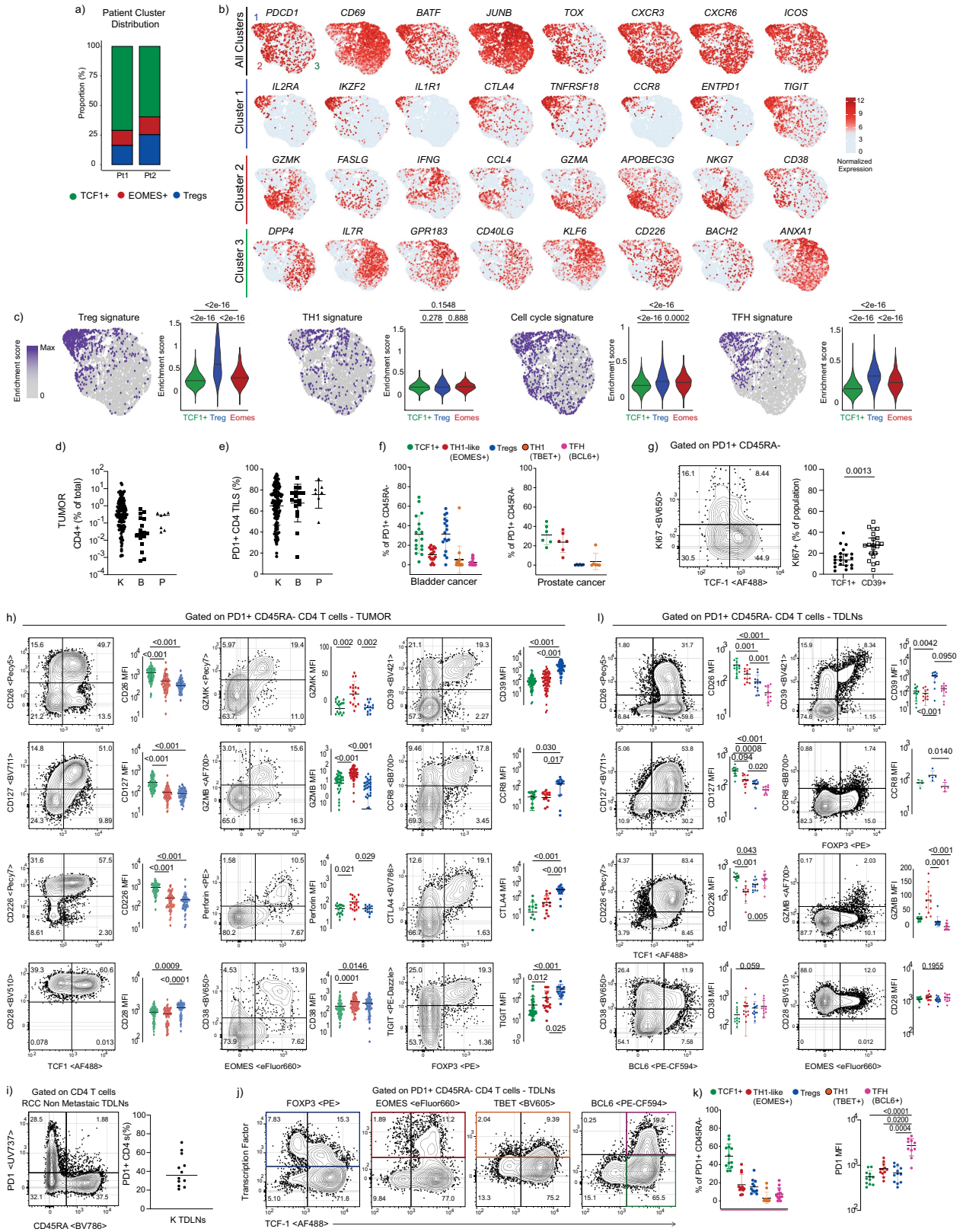

Extended Data Fig. 1 | See next page for caption.

Extended Data Fig. 1 | Phenotypic characterization of PD1 + CD45RA- CD4 T cells in kidney, bladder and prostate cancer patients. a) ScRNAseq analysis of PD1 + CD45RA- CD4 T cells in kidney cancer patients (n = 2). Bar plot showing cluster distribution between patients. b) UMAP projections of selected genes across all clusters. c) VISION GSEA using defined human CD4 T cell lineage (Treg, Th1, Tfh) and proliferation (cell cycle) signatures. UMAP projections show the top 10% scoring cells and the enrichment score for the signature is represented as violin plots for each cluster. Means shown for every violin plot and were analyzed by one-way ANOVA with Tukey's multiple-comparison tests. d-e) Total quantification (d) and frequency of PD1+ (e) CD4 T cell infiltration in kidney (K n = 125), prostate (P n = 6) and bladder (B n = 17) tumors. f) Frequency of activated CD4 T cell populations based on transcription factor expression in human bladder (n = 17) and prostate (n = 6) tumors. g) Representative TCF1 and KI67 expression in activated CD4 T cells infiltrating human kidney tumors (n = 21). Mean ± 95% CI are represented and were analyzed by two-sided unpaired Mann Whitney U test. h) Representative plots of various phenotypic markers expressed in activated CD4 T cells in human kidney tumors. Mean ± s.d. are represented in each summary plot and were analyzed by Kruskal-Wallis test with Dunn's multiple-comparison tests (n = 14–125 kidney cancer patients for each marker). i) Quantification of PD1 + CD4 T cell infiltration in kidney tumor draining lymph nodes, shown as the percent of total CD4 T cells (n = 12). j-k) Representative lineage transcription factor and PD1 expression in PD1 + CD45RA- CD4 T cell populations in kidney tumor draining lymph nodes (n = 9–12). Mean ± s.d. are represented in each summary plot and were analyzed by Kruskal-Wallis test with Dunn's multiple-comparison tests. l) Phenotype of activated CD4 T cells in kidney tumor draining lymph nodes (n = 5–12 patients per marker). Mean ± s.d. are represented in each summary plot and were analyzed by Kruskal-Wallis test with Dunn's multiple-comparison tests. Each point represents an individual patient. The activated populations were defined based on the following gates: Tregs: CD28 + FOXP3 + TBET- EOMES-, EOMES: CD28 + FOXP3- TBET-EOMES +, TFH: CD28 + FOXP3- TBET-EOMES-TCF1 + BCL6 +, Th1: CD28- FOXP3-TBET +, TCF1+lin-: CD28 + FOXP3-TBET-EOMES-TCF1 + BCL6-.

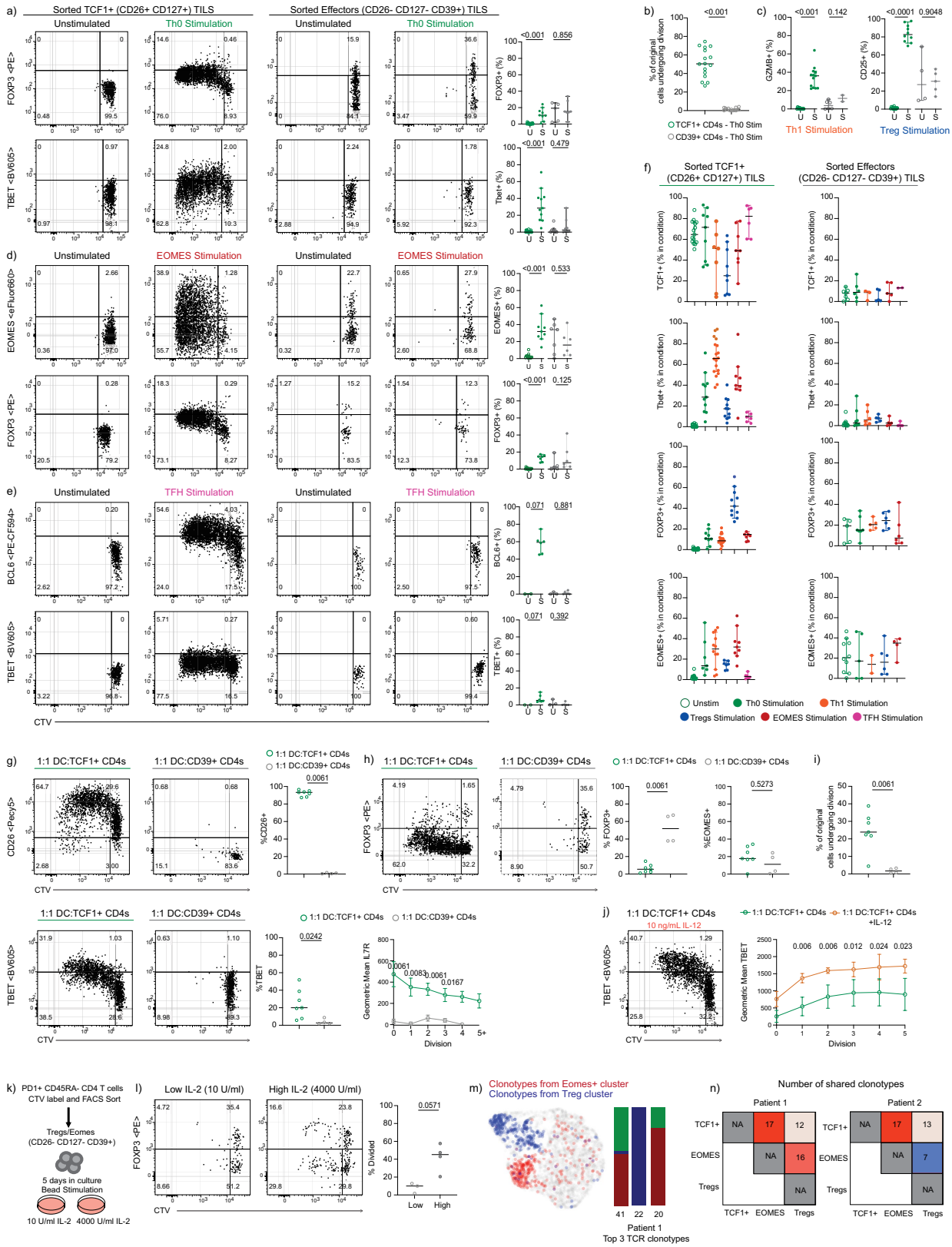

Extended Data Fig. 2 | See next page for caption.

Extended Data Fig. 2 | Tumor PD1 + TCF1+lin- CD4 T cells retain proliferation and differentiation capacity. Representative CTV staining and expression of selected differentiation markers after five days of culturing TCF1+ lin- and CD39 + CD4 T cells in unstimulated (U) or **a)** Th0 (green, TCF1+ n = 11, CD39+ n = 8) **d)** Eomes (red, TCF1+ n = 9, CD39+ n = 6) and **e)** TFH (pink, TCF1+ n = 6, CD39+ n = 6) stimulating conditions. Summary plots show the frequency of cells within each population positive for the indicated marker on day 5. Each point represents an individual patient. Multiple conditions were performed with the same patient depending on cell sorting numbers. Median ± 95% CI are represented and analyzed by two-sided unpaired Mann–Whitney U test. U vs. S within the same population were compared across conditions. b) Frequency of original plated cells undergoing division for TCF1+ or CD39 + CD4 T cells in Th0 conditions. Median is represented and analyzed by two-sided unpaired Mann-Whitney U test. c) Frequency of TCF1+ or CD39 + CD4 T cells expressing the indicated marker on day 5 under Th1 (TCF1+ n = 13, CD39+ n = 2) or Treg stimulation (TCF1+ n = 10, CD39+ n = 5). Median ± 95% CI are represented and analyzed by two-sided unpaired Mann–Whitney U test. f) Summary plots represent the frequency of cells within each sorted population (TCF1+ lin- or CD39+) expressing the indicated transcription factor after 5 days of culture in each of the respective conditions tested. Cytokine stimulation conditions were the following: Th0 (IL-2), Th1 (IL-2 and IL-12), Treg (IL-2, TGF-beta, and anti-IFN gamma), Tfh (Activin A, IL-12), or Eomes (IL2, IL-12, IL-4, aIFNg). g-h) Representative plots of various markers on sorted TCF1+ lin- or CD39 + CD4 T cells after 5-days of 1:1 co-culture with patient matched dendritic cells (n = 7 patients for TCF1+ lin- and n = 4 patients for CD39+). Medians are shown and analyzed by two-sided unpaired Mann–Whitney U test. i) Frequency of original plated cells undergoing division for TCF1+ or CD39 + CD4 T cells after DC co-cultures. Medians are shown and analyzed by two-sided unpaired Mann–Whitney U test. j) Representative plot of TBET expression on TCF1+ lin- CD4 T cells in DC co-cultures with exogenous IL-12 (no IL12 n = 7, IL12 n = 4). Mean ± s.d. are shown and analyzed by two-sided unpaired Mann–Whitney U test between each division. k) Experimental design to test the capacity of PD1 + CD39 + CD4 T cells to proliferate with 4000U/ml of exogenous IL-2. l) Proliferation and FOXP3 expression on sorted CD39 + CD4 T cells after 5-days of CD3/CD2/CD28 bead stimulation with 10U/ml (low, n = 3) or 4000U/ml (high, n = 4) of exogenous IL-2. Medians are shown and analyzed by two-sided unpaired Mann–Whitney U test. m) UMAP projections of the distribution of TCR clonotypes corresponding to cells in the Treg (blue) or Eomes (red) clusters. Summary bar graph shows the cluster distribution of the 3 most dominant TCR clonotypes across all clusters for one patient. The number of cells sharing the respective TCR clonotype is indicated below. n) Correlation matrix showing the number of clonotypes shared by each population in the tumor for both patients.

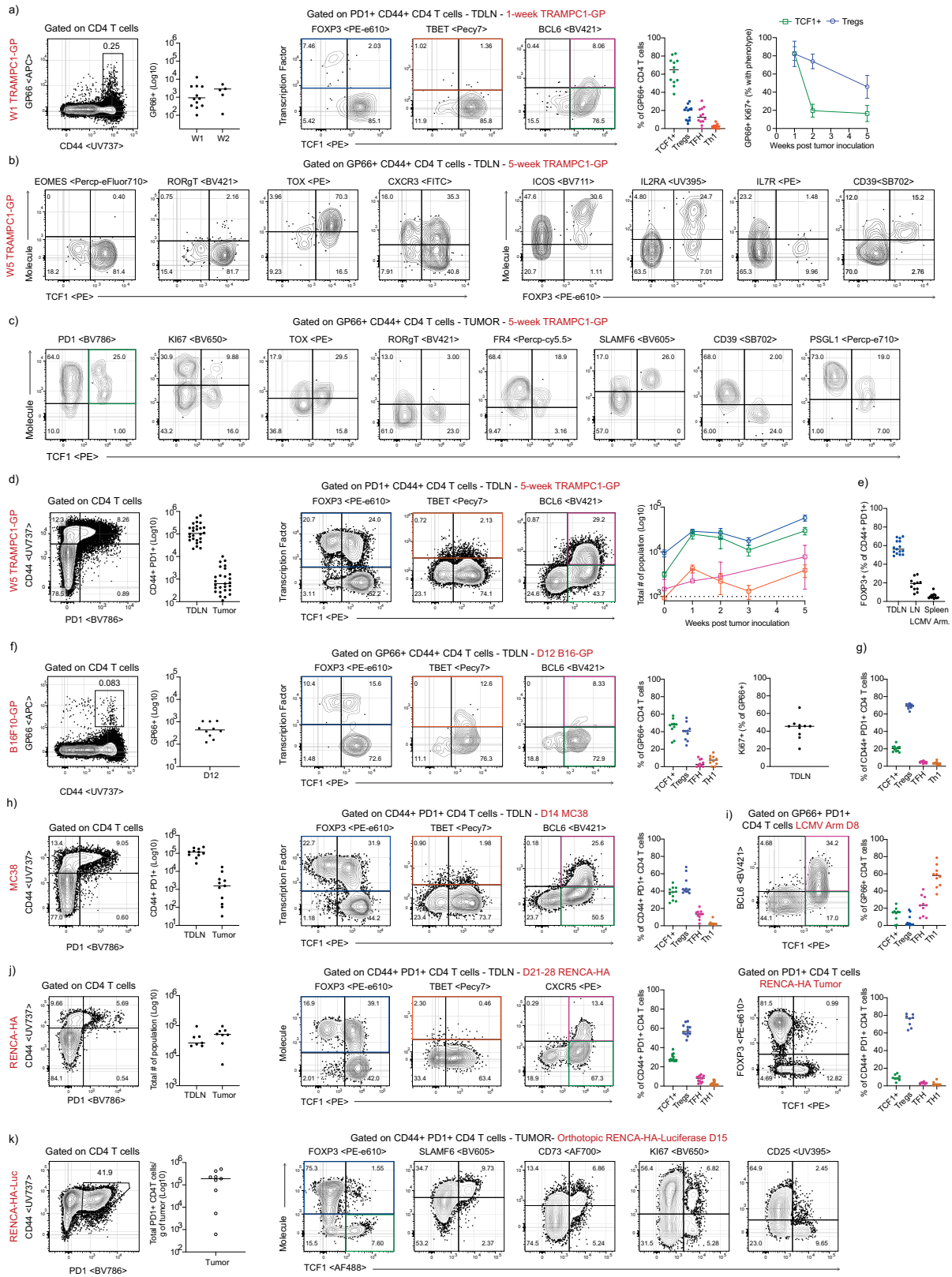

Extended Data Fig. 3 | See next page for caption.

Extended Data Fig. 3 | Tumor specific CD4 T cells activate in TDLNs and rapidly acquire a TCF1+lin phenotype. a) Representative I-A^{b}GP$_{66}$ tetramer staining and phenotype of GP66 + CD4 T cells in TDLNs one-week after TRAMPC1-GP inoculation. b-c) Phenotypic characterization of GP66 + CD4 T cells in TDLNs (b) or tumors (c) of 5-week TRAMPC1-GP bearing mice. Data are representative of 3–5 independent experiments (n > 5 mice for each marker). d) Representative CD44 and PD1 staining and phenotype of bulk PD1 + CD4 T cells in TDLNs of 5-week TRAMPC1-GP bearing mice. Summary plot shows the total numbers of activated (CD44 + PD1 +) CD4 T cell populations in each tissue. Kinetics plot shows the total number of activated CD4 T cells in each phenotype within TDLNs (n > = 5 mice for each timepoint for each individual experiment). e) Frequency of PD1 + CD4 T cells expressing FOXP3 in TDLNs 1-week after tumor inoculation or secondary lymphoid tissues 8-days after LCMV Armstrong infection. Data are representative of 2 independent experiments (n = 5–7 mice per group for each timepoint). f-g) Phenotype of GP66+ (f) or bulk PD1+ (g) CD4 T cells 12-days after B16-GP inoculation in TDLNs. Data are representative of 2 independent experiments (n = 10). h) Representative CD44 and PD1 staining, and phenotype of bulk PD1 + CD4 T cells in TDLNs of day 14 MC38 bearing mice. Data are representative of 2 independent experiments (n = 11). i) Representative TCF1 and BCL6 staining in GP66 + CD4 T cells on D8 LCMV Armstrong infected mice in the spleen. Summary plot shows the frequency of virus specific CD4 T cells in each phenotype. Data are representative of 2 independent experiments (n = 10). j) Phenotype of endogenous CD44 + PD1 + CD4 T cells in subcutaneous D21–28 RENCA-HA TDLNs and tumor (n = 8–12 mice). k) Phenotype of PD1 + CD4 T cells in orthotopic RENCA-HA-Luciferase in tumors 15-days after orthotopic implant (n = 9 mice).

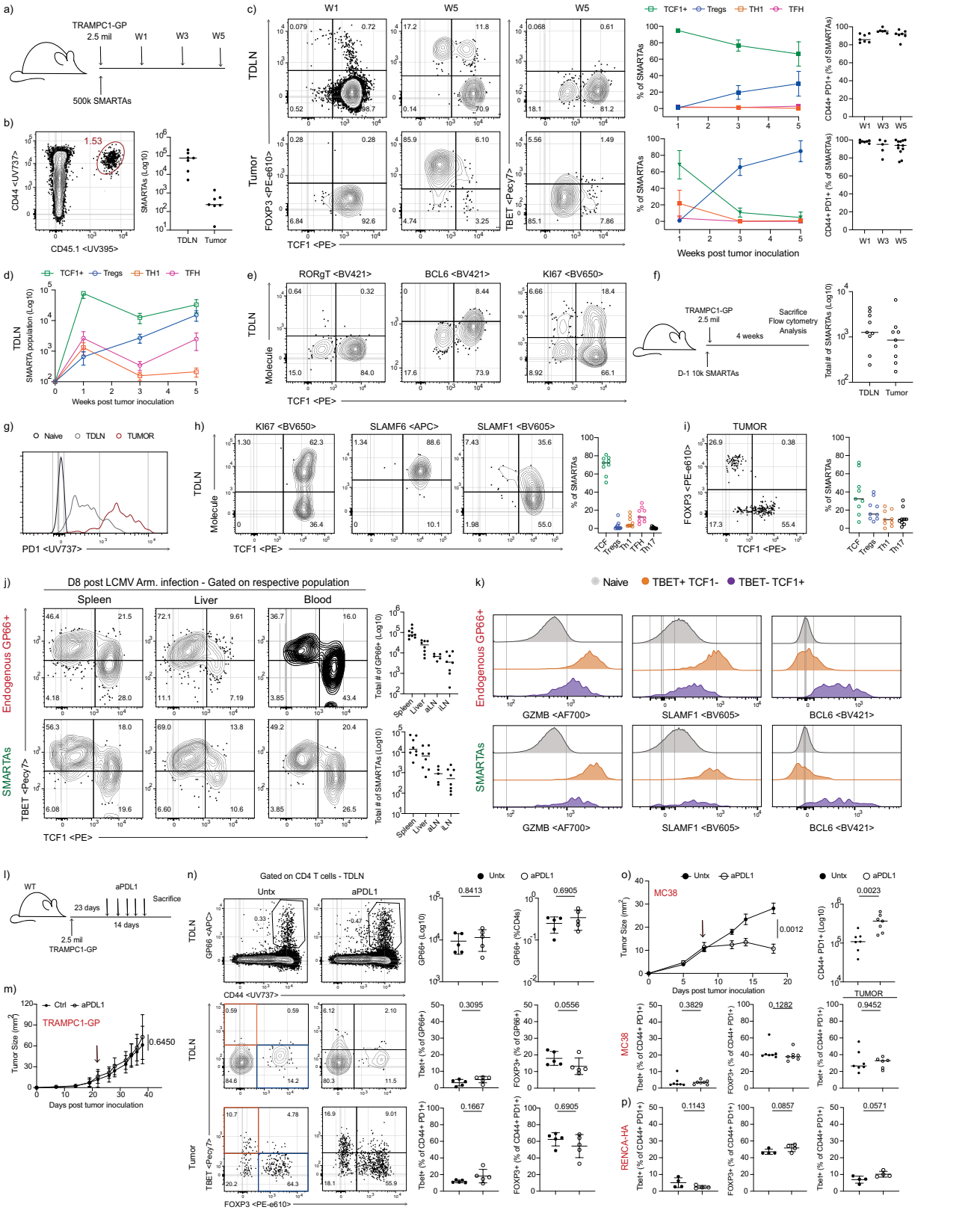

Extended Data Fig. 4 | See next page for caption.

Extended Data Fig. 4 | TCF1+lin- CD4 T cells are stem-like cells that are actively restrained in the tumor response. a) Experimental design to characterize SMARTA differentiation kinetics. b-e) Total numbers and representative phenotype of recovered SMARTAs in TDLNs and tumor 1- to 5-weeks after transfer in TRAMPC1-GP mice. Summary graphs show median or mean ± s.d. Data are representative of 1-2 independent experiments for each timepoint (n = 4–6 mice per group for each timepoint). f) Experimental design and total number of recovered SMARTAs in TDLNs and tumor 4-weeks post transfer. g) Representative histogram of PD-1 expression on recovered SMARTAs in TDLNs and tumor as compared to naïve CD4 T cells. h-i) Phenotypic analysis of SMARTAs in TDLNs and tumor 4-weeks post transfer (n = 9). Medians are shown for each summary plot. j) Representative phenotype of endogenous GP66 + CD4 T cells (top) or transferred SMARTAs (bottom) in the indicated tissue 8 days after LCMV Armstrong infection. Summary plots show median of the total number of GP66+ or SMARTAs in each tissue. k) Representative histograms for Th1 (TBET + TCF1-) and Tfh (TBET- TCF1 + CXCR5 +) populations for the endogenous GP66+ or SMARTAs in the spleen 8 days after LCMV Armstrong infection. Naïve (CD44- PD1-) CD4 T cells are plotted as a reference for each marker. Data are representative of 2 independent experiments (n = 8 recipient mice). l) Experimental design to test how PDL1 therapy affects stem-like CD4 differentiation in TRAMPC1-GP refractory tumor model. m) Tumor kinetics as shown by tumor diameter shown as mean ± s.d. for Untx and aPDL-1 treated mice and analyzed by two-sided unpaired Mann–Whitney U test (n = 5–7 mice per group). n) Phenotype of GP66 + CD4 T cells in TDLNs (top) and tumor (bottom) in Untx or aPDL-1 treated mice 14-days after treatment in TRAMPC1-GP bearing mice. Mean ± s.d. represented and analyzed by two-sided unpaired Mann–Whitney U test (n = 5–7 mice per group). o) Tumor kinetics shown as mean ± s.e.m. and phenotype of PD1 + CD4 T cells for Untx and PDL-1 treated mice in MC38 responsive tumor model. Median shown for phenotype summaries. Statistical comparisons were analyzed by two-sided unpaired Mann–Whitney U test (n = 7 mice per group). p) Phenotype of bulk activated CD4 T cells for untreated and PDL-1 treated mice in RENCA-HA responsive tumor model. Mean ± s.d. are represented and analyzed by two-sided unpaired Mann–Whitney U test (n = 4 mice per group).

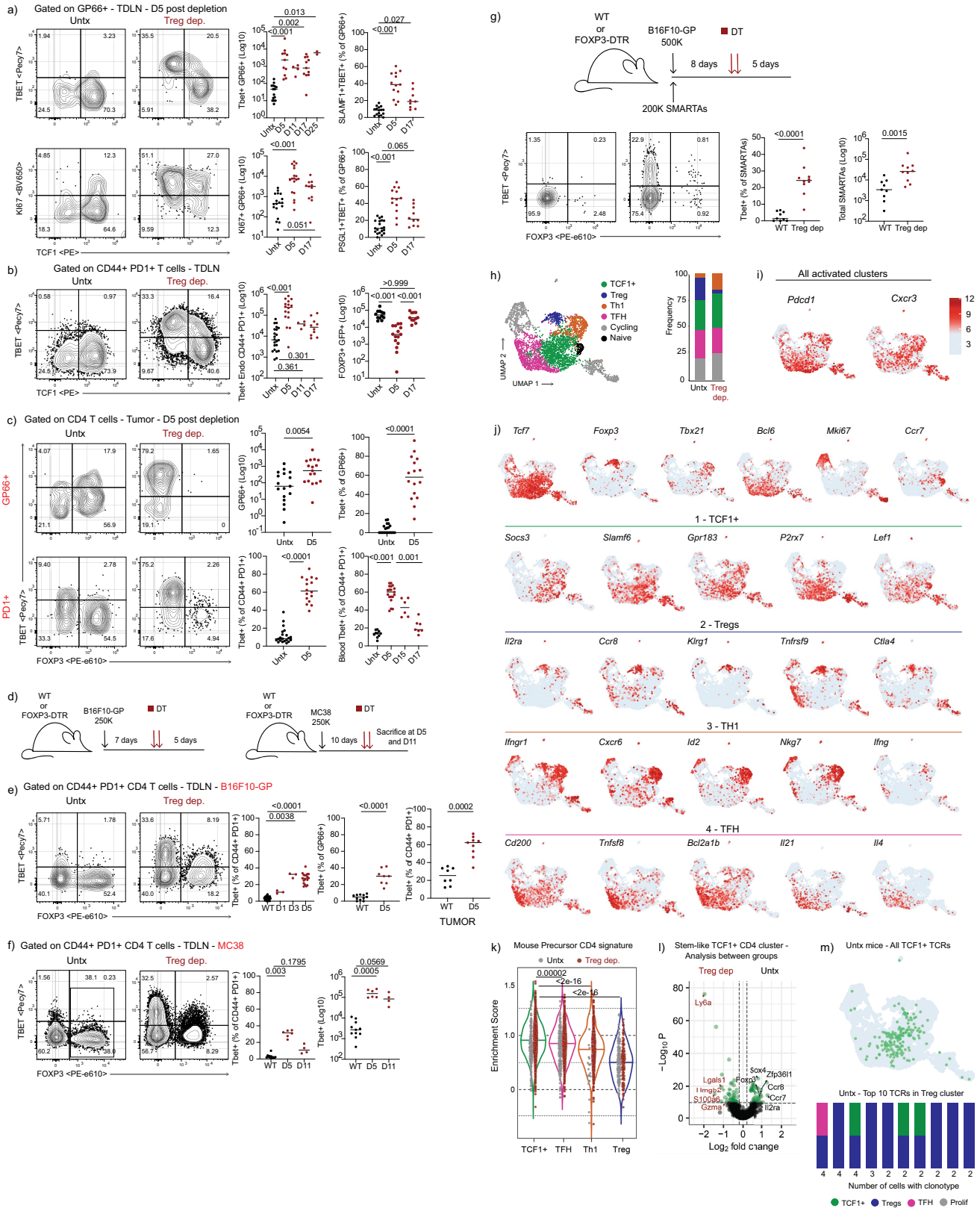

Extended Data Fig. 5 | See next page for caption.

Extended Data Fig. 5 | Phenotypic and transcriptional profiling of antigen specific CD4 T cells generated after Treg depletion in cancer. a-c) Phenotypic analysis of GP66+ and bulk PD1 + CD4 T cells in TDLNs, blood and tumor 5-days after Treg depletion. Median or mean ± s.e.m are shown and analyzed by two-sided unpaired Mann Whitney U or Kruskal-Wallis test with Dunn's multiple-comparison tests when appropriate. Each individual timepoint represents an independent experiment (n = 2–17 mice per group for each time point). d) Schematic of experimental designs for B16F10-GP or MC38 tumors. e-f) Representative TBET by FOXP3 staining of bulk activated CD4 T cells in B16F10-GP (e) or MC38 (f) TDLNs 5-days after Treg depletion. Data represents 3-4 independent experiments (n = 4–5 mice per group for each experiment). Medians are shown and were analyzed by two sided unpaired Mann-Whitney U test or Kruskal-Wallis test with Dunn's multiple-comparison tests when appropriate. g) Schematic of experimental design and phenotypic analysis of transferred SMARTAs in B16F10-GP TDLNs 5-days after Treg depletion. Data represents 2 independent experiments (n = 5 mice per group). Medians are represented in each summary plot and were analyzed by two-sided unpaired Mann-Whitney U test. h) ScRNAseq analysis of bulk activated (CD44 + PD1 +) CD4 T cells sorted from TDLNs of Untx or Treg depleted TRAMPC1-GP mice 5-days after depletion (n = 4-12 pooled mice per group). Naïve (CD44- PD1-) CD4 T cells were included as a control. UMAP projection and cluster distribution of activated CD4 T cells in TDLNs for both groups. i-j) Normalized expression of transcription factors and selected genes defining each cluster. k) VISION GSEA analysis using a signature from precursor TCF1+ BCL6low CD4 T cells from chronic LCMV infection for Untx and Treg depleted mice. Mean is represented in each violin and were analyzed by one-way ANOVA with Tukey's multiple comparison tests. l) Transcriptional comparison of stem-like CD4 T cell cluster between groups. Volcano plots show fold change versus -log(p-value) for each gene. m) UMAP projection of the distribution of all the TCR clonotypes in the TCF1+ stem-like cluster in untreated mice (top). Cluster distribution of the 10 most dominant TCR clonotypes belonging to the Treg cluster in Untx mice. The number of cells sharing the respective TCR clonotype is indicated below (bottom).

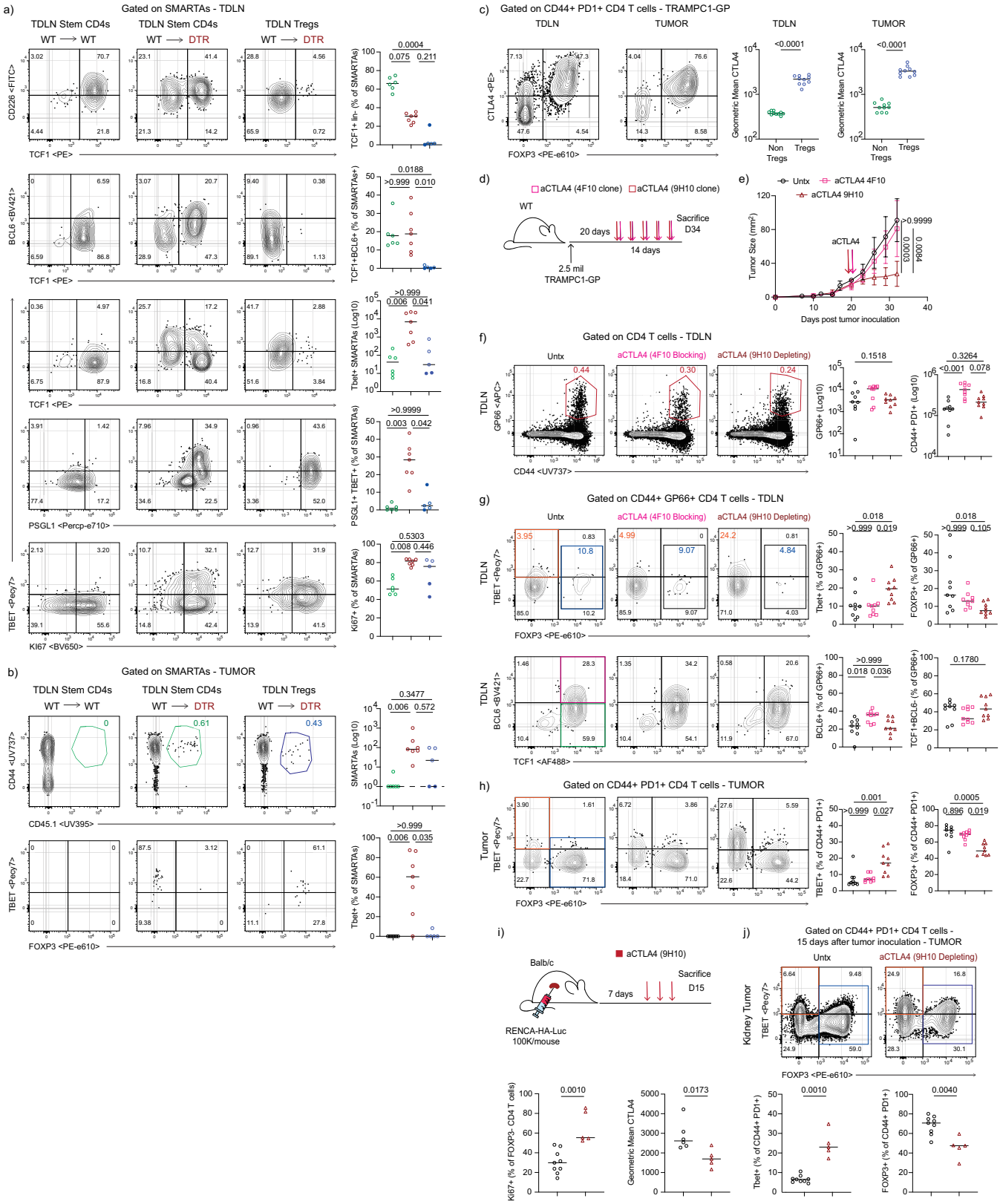

Extended Data Fig. 6 | See next page for caption.

Extended Data Fig. 6 | Stem-like CD4 T cells are the source of Th1 cells in response to Treg depletion and aCTLA4 therapy. a-b) Phenotypic analysis of recovered stem and Treg SMARTAs in TDLNs (a) and tumors (b) 7 days after transfer in WT or Treg depleted (DTR) recipients for each condition. Medians are represented in each summary graph and analyzed by Kruskal-Wallis test with Dunn's multiple-comparison tests. Data are representative of 2 independent experiments (n = 13 for stem-like and n = 5 for Tregs). c) Representative FOXP3 and CTLA4 staining with accompanying CTLA4 geometric MFI in TDLNs and tumors in TRAMPC1-GP bearing mice. Medians are shown and analyzed by two sided unpaired Mann-Whitney U test (n = 10 mice). d) Experimental design to test how Tregs suppress stem-like differentiation through CTLA4 in TRAMPC1-GP bearing mice. e) Tumor kinetics shown as mean tumor diameter ± s.d. in untreated (n = 9), aCTLA4 4F10 (n = 9), or aCTLA4 9H10 (n = 9) mice and analyzed by Kruskal-Wallis test with Dunn's multiple-comparison tests. f-g) Representative f) GP66 staining and g) phenotype of tumor specific CD4 T cells in TDLNs in each treatment group. h) Phenotype of bulk PD1 + CD4 T cells for each treatment group in tumors. Medians are represented in each summary graph and were analyzed by Kruskal-Wallis test with Dunn's multiple-comparisons tests (n = 9 for each group). i) Experimental design to test the effects of aCTLA4 therapy in orthotopic RENCA-HA-Luciferase mice. j) Phenotype analysis of bulk PD1 + CD4 T cells in the tumor for untreated or 9H10 CTLA4 treated orthotopic RENCA-HA-Luc mice. Medians are shown and were analyzed by two sided unpaired Mann-Whitney U test (n = 9 for Untx and n = 5 for 9H10 aCTLA4 group).

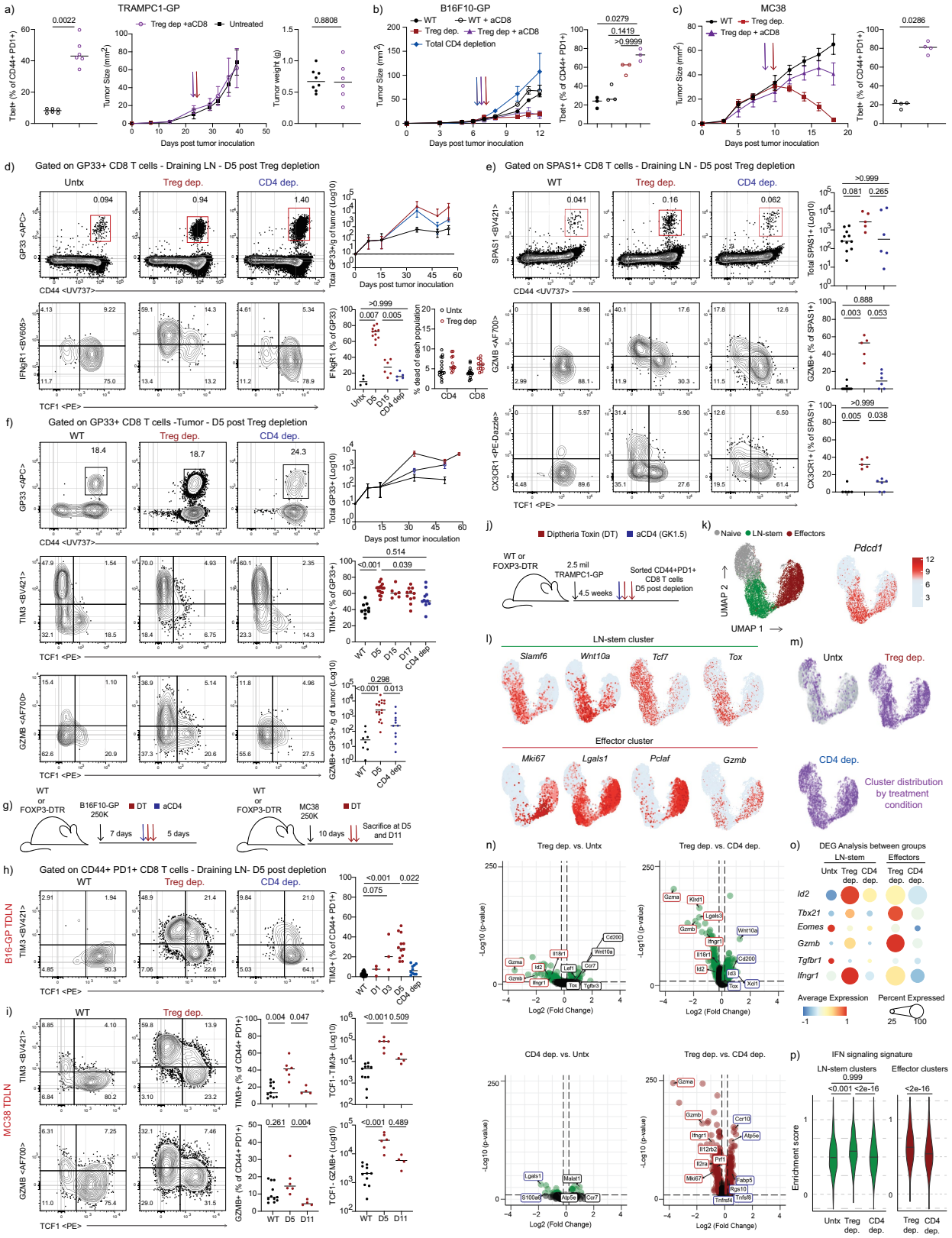

Extended Data Fig. 7 | See next page for caption.

Extended Data Fig. 7 | CD4 T cell help is required for effector CD8 differentiation in TDLNs. a-c) Th1 differentiation and tumor growth kinetics shown as mean ± s.d. for a) TRAMPC1-GP (Untx n = 8, aCD8 n = 6), b) B16F10-GP (n = 3 mice per group) and c) MC38 tumors (n = 4 mice per group) for Untx mice, Treg depleted mice, total CD4-depleted mice (GK1.5 clone), and combination of Treg and CD8 T cell (Lyt3.2 clone) depleted mice. Medians shown in summary plots. Statistical comparisons were performed using two-sided unpaired Mann-Whitney U test or Kruskal-Wallis test with Dunn's multiple-comparison tests when appropriate. d-e) Phenotypic analysis of d) GP33+ and e) SPAS1 + CD8 T cells in TRAMPC1-GP TDLNs 5-days after Treg or total CD4 T cell depletions. f) Phenotype of GP33 + CD8 T cells in tumor 5-days after Treg or total CD4 T cell depletion. Every time point represents an independent experiment (n = 5–17 mice per group). Medians or mean ± s.e.m are represented in each summary plot and were analyzed by Kruskal-Wallis test with Dunn's multiple-comparison tests. g) Schematic of experimental designs. h-i) Phenotypic analysis of bulk activated CD8 T cells in h) B16F10-GP i) or MC38 TDLNs after Treg or total CD4 depletion. Summary plots show total number or frequency of activated CD8 T cells expressing the indicated marker at the respective time points (n = 3–7 mice per group per timepoint for each independent experiment). Medians are represented in each summary plot and were analyzed by Kruskal-Wallis test with Dunn's multiple-comparison tests. j) Experimental design. ScRNAseq of sorted naïve and activated (CD44 + PD1 +) CD8 T cells from TDLNs of Untx, Treg depleted, and total CD4 depleted TRAMPC1-GP bearing mice 5-days after depletion (n = 4–12 pooled mice per group). k-m) Cluster distributions and UMAP projections of normalized expression of genes defining the naïve, LN-stem, and effector CD8 clusters in all conditions. n) Transcriptional comparisons of LN-stem and effector CD8 T cells between groups. Volcano plots show fold change versus -log(p-value) for each gene within each respective comparison. o) Transcriptional comparison of selected genes across LN-stem (green) and effector (red) clusters between Untx, Treg depleted, and CD4 depleted groups. The color and size of the circles represent the normalized expression and proportion of cells expressing that gene, respectively. p) VISION GSEA using an IFN signaling signature. Signature enrichment score is represented as violin plots for LN-stem (green) and effector (red) clusters in the respective groups. Mean is represented in each violin and were analyzed by one-way ANOVA with Tukey's multiple comparison tests (n = 4–12 pooled mice per group).

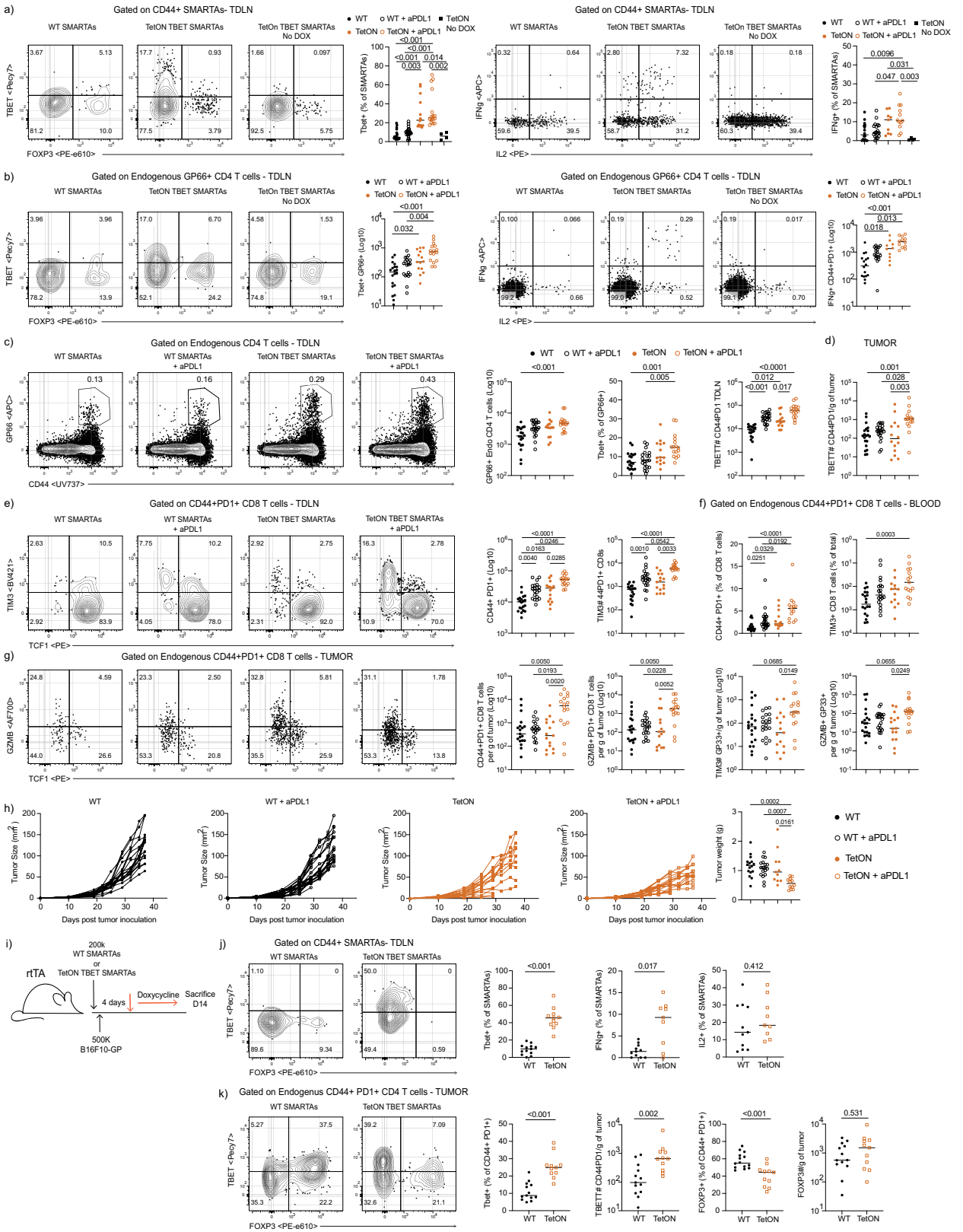

Extended Data Fig. 8 | See next page for caption.

Extended Data Fig. 8 | Localized Th1 response is sufficient to induce endogenous stem-like to Th1 differentiation and improve response to immunotherapy in the presence of Tregs. a) Phenotype and cytokine production after GP61-77 stimulation of transferred SMARTAs across all groups in TDLNs. Summary plots show the frequency of SMARTAs expressing TBET and producing IFNg. b) Phenotype and cytokine production after GP61-77 stimulation of endogenous GP66 + CD4 T cells in TDLNs for each group. Summary plots show the total number of GP66 + CD4 T cells expressing TBET and producing IFNg. c-d) Representative GP66 staining in TDLNs for each group and summary of the phenotype of endogenous bulk and GP66 + CD4 T cell expressing Tbet in TDLNs and tumors. e-h) Phenotype of endogenous bulk activated (CD44 + PD1 +) or GP33 + CD8 T cells in e) TDLNs, f) blood and g) tumor for each group. Data represents 3 independent experiments. a-g) Median are represented in each summary plot and were analyzed by Kruskal Wallis test with Dunn's multiple-comparison tests (n = 4–6 mice per group for each experiment). h) Individual tumor growth kinetics of TRAMPC1-GP mice after SMARTA transfer and tumor weights at endpoint for each group. Summary tumor weights represented as grams for each group. Medians are shown and were analyzed by Kruskal Wallis test with Dunn's multiple-comparison tests (n = 4–6 mice per group for each independent experiment). i) Experimental design. j) Phenotype and cytokine production after GP61-77 stimulation of transferred WT or TetON TBET SMARTAs in TDLNs. k) Phenotype of endogenous PD1 + CD4 T cells in the tumor. Summaries show the frequency and number of Th1 and Tregs infiltrating the tumor. Data represents two independent experiments and were analyzed by two-sided unpaired Mann Whitney U test (n = 5–7 mice per group for each experiment).

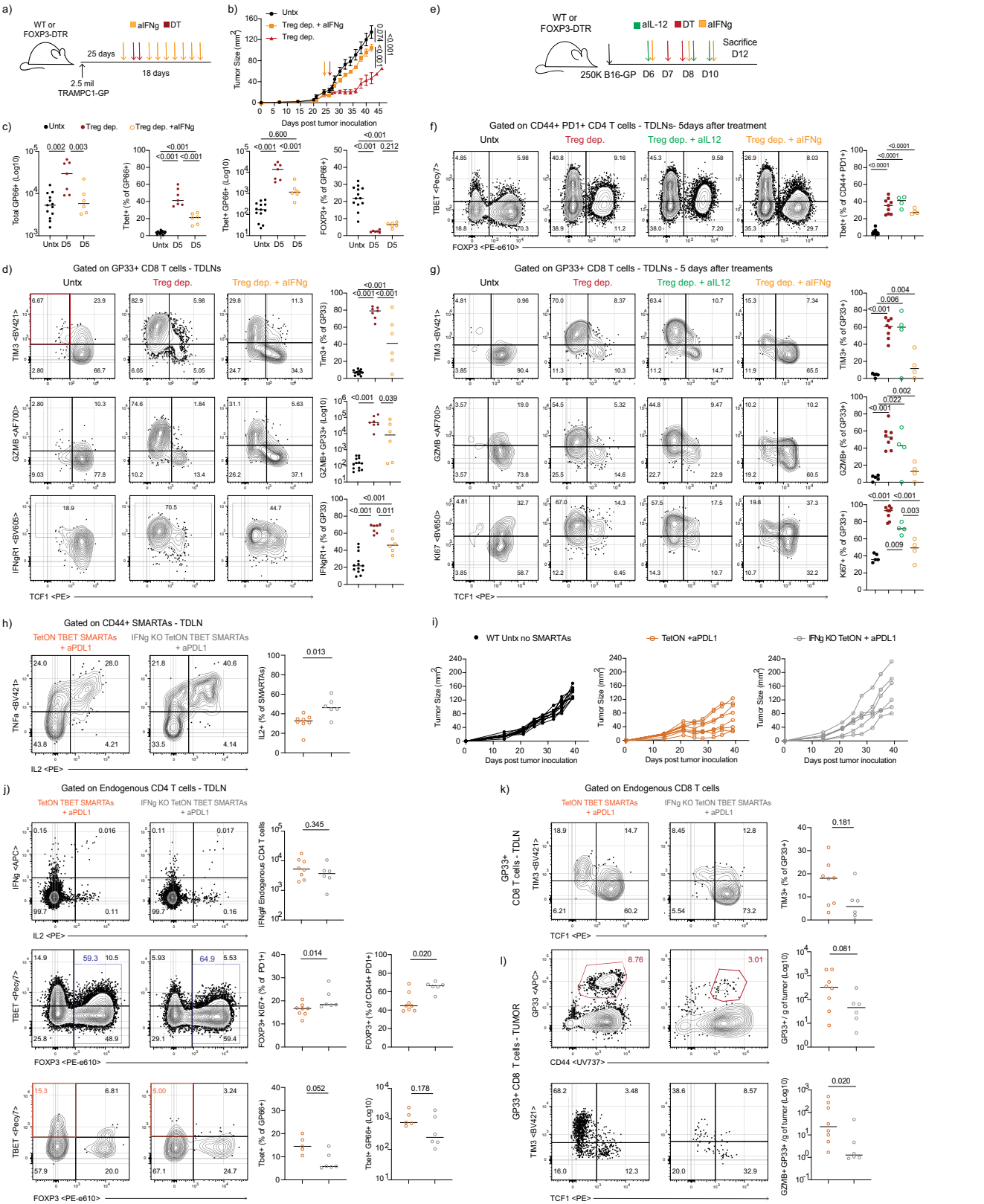

Extended Data Fig. 9 | See next page for caption.

Extended Data Fig. 9 | Th1-derived IFNg is required for effective anti-tumor immunity. a) Experimental design for systemic IFNg block in TRAMPC1-GP mice. b) TRAMPC1-GP tumor kinetics shown as tumor diameter. Data are representative of 2 independent experiments. Mean ± s.e.m. shown and were analyzed by Kruskal Wallis test with Dunn's multiple comparison tests between groups (Untx n = 11, Treg dep. n = 13, Treg dep + aIFNg n = 8). c) Total numbers and phenotypic analysis of tumor specific GP66 + CD4 T cells in TDLNs 5-days after Treg depletion and IFNg block. d) Phenotypic analysis of GP33 + CD8 T cells in TDLNs in TRAMPC1-GP bearing mice after 5-days of Treg depletion and IFNg block. Medians are represented in each summary plot and were analyzed by One-way ANOVA test with Tukey's multiple comparison tests between groups (n = 6-13 mice per group). e) Experimental design for systemic IFNg and IL-12 block in B16-F10-GP mice. f-g) Phenotypic analysis of CD44 + PD1 + CD4 or GP33 + CD8 T cells in TDLNs of B16F10-GP bearing mice 5-days after each depletion or cytokine blocks. Medians are represented in each summary plot and were analyzed by One-way ANOVA test with Tukey's multiple comparison tests between groups (n = 4–8 mice per group). h) Cytokine production after GP61-77 stimulation of transferred TetON or IFNg KO TetON SMARTAs in TDLNs of TRAMPC1-GP mice. i) Individual tumor growth kinetics of TRAMPC1-GP mice after SMARTA transfer for each group. j) Phenotype and cytokine production (GP61-77 peptide stimulation) of endogenous GP66+ or bulk PD1 + CD4 T cells in TDLNs of mice receiving WT or IFNg KO TetON TBET SMARTAS. k-l) Phenotypic analysis of GP33 + CD8 T cells in TDLNs (k) and tumor (l) of mice receiving WT or IFNg KO TetON TBET SMARTAS. Median are represented in each summary plot and were analyzed by two-sided unpaired Mann Whitney U test between groups. (n = 6–8 mice per group).

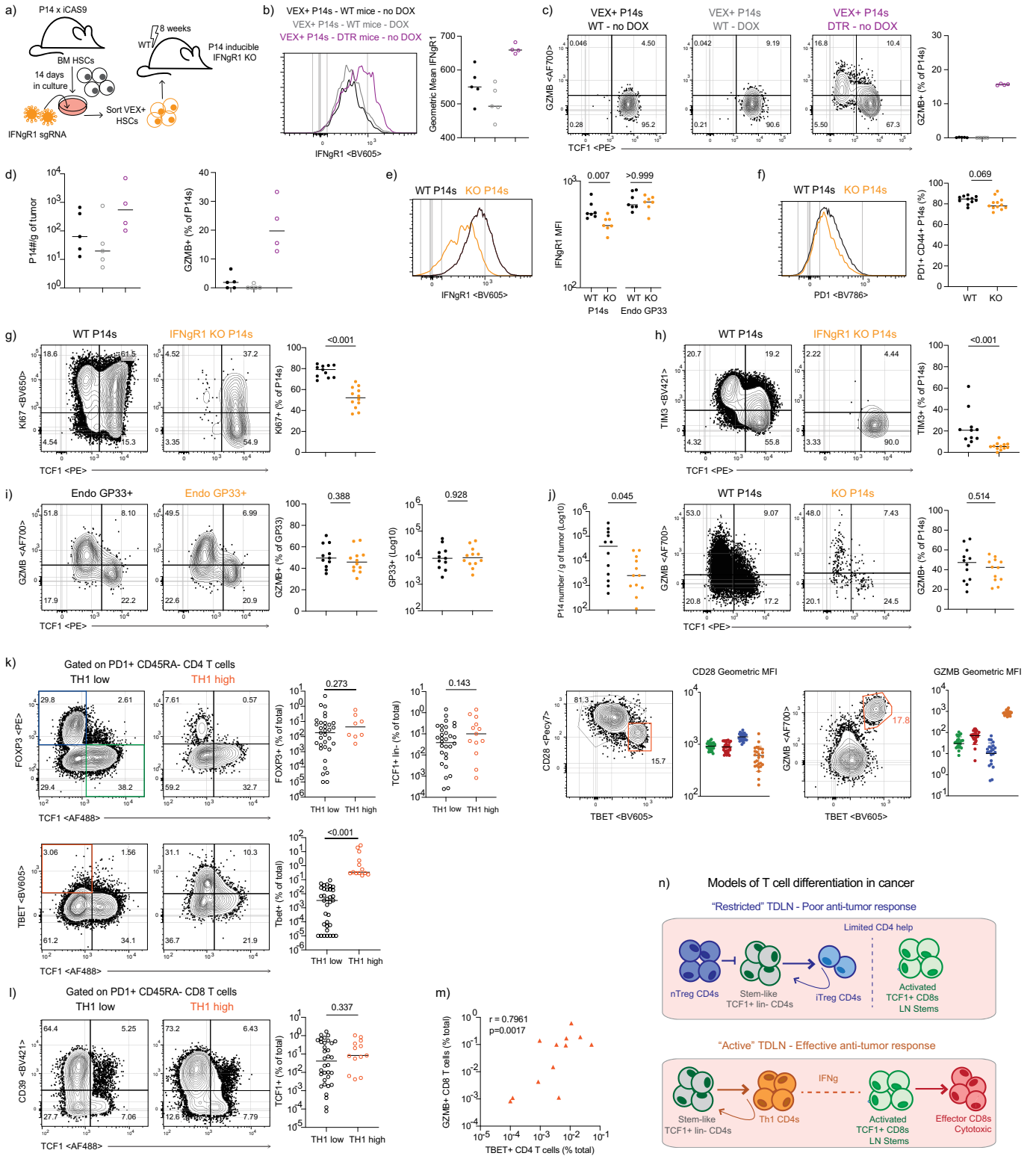

Extended Data Fig. 10 | See next page for caption.

Extended Data Fig. 10 | IFNg is intrinsically required for tumor specific CD8 LN-stem to effector differentiation. a) Schematic to make IFNgR1 KO P14s using an HSC BM chimera lentiviral system. b-d) Phenotypic analysis of transferred VEX+ P14s in WT mice with and without doxycycline administration and Treg depleted (DTR) mice without doxycycline treatment in TDLNs and tumor. Medians are represented in each summary plot (n = 4–5 mice per group). e-f) Representative flow cytometry stain of IFNgR1 and PD1 expression in WT and KO P14s after transfer into FOXP3-DTR TRAMPC1-GP mice. Endogenous GP33 + CD8 T cells in each respective mouse are included as a comparison. Medians are represented in each summary plot from one representative experiment and analyzed by two-sided unpaired Mann Whitney U test between WT and KO (n = 7 mice). g-h) Phenotype of transferred WT and IFNgR1 KO P14s in TDLNs 5-days after Treg depletion. i) Total number and phenotypic analysis of endogenous GP33 + CD8 T cell numbers in TDLNs in mice with transferred WT and KO P14s. j) P14 number and phenotype in the tumor 5-days after Treg depletion. Data are representative of 2 independent experiments (n = 5–6 mice per group for each experiment). Median are represented in each summary plot and were analyzed by two-sided unpaired Mann-Whitney U test. k) Representative phenotype of activated (PD1 + CD45RA-) CD4 T cells in primary tumors upon surgical resection in a cohort of 47 kidney cancer patients that received immunotherapy. Patients where stratified based on the % of total TBET + PD1 + CD4 T cells in the resected primary tumors prior to therapy. l) Representative phenotype of activated (PD1 + CD45RA-) CD8 T cells in Th1 low and Th1 high patients. Medians are represented and analyzed by two-sided unpaired Mann-Whitney U test (n = 47 kidney cancer patients). m) Spearman correlation between TBET + CD4 T cells and effector GZMB + CD8 T cell populations as a percent of total cells in non-metastatic draining lymph nodes from kidney cancer patients (n = 12). n) **Proposed models of T cell differentiation states in TDLNs. Restricted TDLN state**. Tregs actively suppress stem-like CD4 T cells, preventing their differentiation into Th1 cells and promoting iTreg differentiation. Minimal CD4 T cell help is provided in this state and CD8 T cells are maintained in an activated stem-like state in TDLNs. Anti-tumor response is not optimal, and tumor outcompetes the T cell response. **Active TDLN state**. In the absence of Treg suppression stem-like CD4 T cells undergo Th1 differentiation. Th1 CD4s secrete IFNg which promotes stem-like to effector CD8 T cell differentiation. Anti-tumor effector response is optimal, and tumor is controlled. Stem-like CD4 T cell differentiation can be targeted and stimulated to generate Th1 cells in the presence of Tregs. Stem to Th1 CD4 differentiation is then sufficient to switch between active and restricted states and rescue response to immunotherapy.

nature portfolio

Corresponding author(s): Haydn Kissick

Last updated by author(s): Jun 18, 2024

Reporting Summary

Nature Portfolio wishes to improve the reproducibility of the work that we publish. This form provides structure for consistency and transparency in reporting. For further information on Nature Portfolio policies, see our Editorial Policies and the Editorial Policy Checklist.

Statistics

For all statistical analyses, confirm that the following items are present in the figure legend, table legend, main text, or Methods section.

n/a	Confirmed	
☐	☒	The exact sample size (*n*) for each experimental group/condition, given as a discrete number and unit of measurement
☐	☒	A statement on whether measurements were taken from distinct samples or whether the same sample was measured repeatedly
☐	☒	The statistical test(s) used AND whether they are one- or two-sided *Only common tests should be described solely by name; describe more complex techniques in the Methods section.*
☒	☐	A description of all covariates tested
☐	☒	A description of any assumptions or corrections, such as tests of normality and adjustment for multiple comparisons
☐	☒	A full description of the statistical parameters including central tendency (e.g. means) or other basic estimates (e.g. regression coefficient) AND variation (e.g. standard deviation) or associated estimates of uncertainty (e.g. confidence intervals)
☐	☒	For null hypothesis testing, the test statistic (e.g. *F*, *t*, *r*) with confidence intervals, effect sizes, degrees of freedom and *P* value noted *Give P values as exact values whenever suitable.*
☒	☐	For Bayesian analysis, information on the choice of priors and Markov chain Monte Carlo settings
☒	☐	For hierarchical and complex designs, identification of the appropriate level for tests and full reporting of outcomes
☒	☐	Estimates of effect sizes (e.g. Cohen's *d*, Pearson's *r*), indicating how they were calculated

Our web collection on statistics for biologists contains articles on many of the points above.

Software and code

Policy information about availability of computer code

Data collection	Flow cytometry data were collected on a Symphony instrument A5 with FACSDiva software v9.0 (BD).
Data analysis	Flow cytometry data were analyzed on Flowjo v10.7.1(TreeStar) and statistical analysis was performed on Prism v9.00 (GraphPad). ScRNAseq alignment was performed using CellRanger v3.1, and analysis was performed using R studio v4.1.2, Seurat v4.0.3, VISION v3.0 and base R packages that were updated to most current version. NicheNet analysis was performed using nichenetr 1.0.0. TCR alignment to V,D,J gene segments was performed using using MixCR v3.0. sgRNA was designed using CHOPCHOP design tool.

For manuscripts utilizing custom algorithms or software that are central to the research but not yet described in published literature, software must be made available to editors and reviewers. We strongly encourage code deposition in a community repository (e.g. GitHub). See the Nature Portfolio guidelines for submitting code & software for further information.

Data

Policy information about availability of data

All manuscripts must include a data availability statement. This statement should provide the following information, where applicable:

- Accession codes, unique identifiers, or web links for publicly available datasets
- A description of any restrictions on data availability
- For clinical datasets or third party data, please ensure that the statement adheres to our policy

Raw fastq files and associated scRNA sequencing have been uploaded to the NCBI Gene Expression Omnibus (GEO) database under identifier XXX. Other relevant data are available from the corresponding author upon reasonable request.

Research involving human participants, their data, or biological material

Policy information about studies with human participants or human data. See also policy information about sex, gender (identity/presentation), and sexual orientation and race, ethnicity and racism.

Reporting on sex and gender	No hypothesis was tested relating to the sex or gender of patients, and this characteristic of the patient from whom the sample was collected was not delivered as part of the de-identified information on each sample. These data can be retrieved if required.
Reporting on race, ethnicity, or other socially relevant groupings	No data on race, ethnicity or other socially relevant characteristics where analyzed in this study.
Population characteristics	No data regarding patient race
Recruitment	Patients undergoing surgery at Emory University Hospital were recruited in accordance with approved IRB protocol (number here), and all patients provided informed consent. Patient tumour samples were collected immediately after undergoing partial or radical nephrectomy or prostatectomy or undergoing transurethral resection of a bladder tumor (TURBT).
Ethics oversight	Emory University Institutional Review Board protocol (IRB00055316), with all patients providing informed consent.

Note that full information on the approval of the study protocol must also be provided in the manuscript.

Field-specific reporting

Please select the one below that is the best fit for your research. If you are not sure, read the appropriate sections before making your selection.

☒ Life sciences ☐ Behavioural & social sciences ☐ Ecological, evolutionary & environmental sciences

For a reference copy of the document with all sections, see nature.com/documents/nr-reporting-summary-flat.pdf

Life sciences study design

All studies must disclose on these points even when the disclosure is negative.

Sample size	For mouse studies, sample sizes were based on those used in previous and preliminary studies from our lab, but group sizes were not preselected. Sample sizes of n=3-12 mice were chosen to allow for determination of at least a ~50% difference relative to control populations. If experiments had higher levels of variance, we performed additional repeats to account for this variance. For human studies, sample size for each experiment is described in each figure and was based on the availability of adequate samples. No sample size calculations were performed prior to the study.
Data exclusions	No data were excluded.
Replication	For human functional experiments, no replication was performed on individual patient specimens within the same condition given limited sample availability. However, several conditions were performed from the same patient with similar results. Additionally, analyses were performed over several batches of patients with consistent results within each condition. For mouse experiments, details of the number of mice and experiment replications are in figure legends.
Randomization	Tumor experiments with antibody treatments or depletions were randomized by distributing recipient mice based on tumor size at time of treatment and selecting recipient mice at random for each group.
Blinding	The investigators were not blinded to group allocation during data collection or analysis.

Reporting for specific materials, systems and methods

We require information from authors about some types of materials, experimental systems and methods used in many studies. Here, indicate whether each material, system or method listed is relevant to your study. If you are not sure if a list item applies to your research, read the appropriate section before selecting a response.

Materials & experimental systems

n/a	Involved in the study
☐	☒ Antibodies
☐	☒ Eukaryotic cell lines
☒	☐ Palaeontology and archaeology
☐	☒ Animals and other organisms
☒	☐ Clinical data
☒	☐ Dual use research of concern
☒	☐ Plants

Methods

n/a	Involved in the study
☒	☐ ChIP-seq
☐	☒ Flow cytometry
☒	☐ MRI-based neuroimaging

Antibodies

Antibodies used

The antibodies used for flow cytometry are detailed in Ext. Data Table 2.
The following antibodies were used for depletion or blocking experiments:
Mouse anti-CD8b (BioXCell, Cat#BE0223; Clone#Lyt3.2), Mouse anti CD4 (BioXCell, Cat#BE0003-1, Clone#GK1.5), Mouse anti IL-12p40 (BioXCell, Cat#BE0051, Clone#C17.8), Mouse anti IFNγ (BioXCell, Cat#BE0055, Clone#XMG1.2), Mouse anti PD-L1 (BioXCell, Cat#BP0101, Clone#10F.9G2), Mouse aCTLA4 blocking antibody (BioXcell, Cat#BP0032, Clone#UC10-4F10-11), Mouse aCTLA4 depleting antibody (BioXcell, Cat#BE0131, Clone#9H10).

Validation

The specificities of primary antibodies used in this study are widely used and well validated by the manufacturers by flow cytometry. The validation information is available through the manufacturers' websites for each catalog number provided in Ext. Data Table 2.

Eukaryotic cell lines

Policy information about cell lines and Sex and Gender in Research

Cell line source(s)

TRAMPC1 cell line expressing full length LCMV glycoprotein (GP) were made using lentiviral transduction from ATCC. B16-F10 was obtained from ATCC and the full length LCMV glycoprotein (GP) was made by lentiviral transduction by Rafi Ahmed's lab. B16F10-GP cell line was a gift from Rafi Ahmed's lab. MC38 cell line was obtained from ATCC. RENCA cell line was obtained from ATCC and Influenza HA was added through lentiviral transduction. RENCA-HA-Luciferase was made by an additional transduction of a lentiviral plasmid containing luciferase and neomycin. Cells were selected on neomycin resistance for 10 days.

Authentication

The cell lines were all obtained from ATCC and no further verification has been performed

Mycoplasma contamination

All cell lines are tested anually for mycoplasma contamination and were negative as of the 2024.

Commonly misidentified lines
(See ICLAC register)

No commonly misidentified cell lines were used.

Animals and other research organisms

Policy information about studies involving animals; ARRIVE guidelines recommended for reporting animal research, and Sex and Gender in Research

Laboratory animals

All mice were used and maintained in accordance with National Institutes of Health and the Emory University Institutional Animal Care and Use Committee guidelines. Mice were housed with light cycles between 7am and 7pm, temperature of 72F and humidity between 40% and 50%. C57BL/6J mice (#000664), Pep Boy mice (B6.SJL-Ptprca Pepcb/BoyJ, #002014), and BALB/cJ (#000651) were purchased from Jackson laboratories between the ages of 7-10 weeks. LCMV DbGP33-specific TCR transgenic P14 were a gift from Rafi Ahmed's lab and were bred and maintained at Emory University. LCMV GP66-77 specific SMARTA mice (#030450) were purchased from Jackson laboratories and were bred and maintained at Emory University. FOXP3-DTR mice (DEREG, #032050-JAX) expressing the human diphtheria toxin receptor and the GFP reporter [1] were used for Treg depletion experiments. rtTA (Rosa26-CAGs-rtTA3 knock-in, #029627) mice were bred in house and crossed with transgenic SMARTA mice for Tbet overexpression experiments. iCas9 (B6;129S4-Gt(ROSA)26Sortm1(rtTA*M2)Jae Col1a1tm1(tetO-cas9)Sho/J, #029415) mice were bred in house and crossed with rtTA mice for inducible knockout experiments.

Wild animals

The study did not involve wild animals.

Reporting on sex

For tumor experiments, male C57BL/6J mice were strictly used for the TRAMPC1-GP cell line due to testosterone growth dependency of the cell line, while female C57BL/6J mice were primarily used for B16-GP and MC38 experiments. Female BALB/cJ mice were

primarily used for RENCA-HA subcutaneous and orthotopic experiments. Both male and female mice were included in all analyses reported in this manuscript and the sex is reported in the methods.

Field-collected samples: The study did not involve samples collected from the field.

Ethics oversight: Animal experiments were conducted and designed in accordance with National Institutes of Health and the Emory University Institutional Animal Care and Use Committee guidelines and approved under PROTO201800261 .

Note that full information on the approval of the study protocol must also be provided in the manuscript.

Plants

Seed stocks: *Report on the source of all seed stocks or other plant material used. If applicable, state the seed stock centre and catalogue number. If plant specimens were collected from the field, describe the collection location, date and sampling procedures.*

Novel plant genotypes: *Describe the methods by which all novel plant genotypes were produced. This includes those generated by transgenic approaches, gene editing, chemical/radiation-based mutagenesis and hybridization. For transgenic lines, describe the transformation method, the number of independent lines analyzed and the generation upon which experiments were performed. For gene-edited lines, describe the editor used, the endogenous sequence targeted for editing, the targeting guide RNA sequence (if applicable) and how the editor was applied.*

Authentication: *Describe any authentication procedures for each seed stock used or novel genotype generated. Describe any experiments used to assess the effect of a mutation and, where applicable, how potential secondary effects (e.g. second site T-DNA insertions, mosiacism, off-target gene editing) were examined.*

Flow Cytometry

Plots

Confirm that:

☒ The axis labels state the marker and fluorochrome used (e.g. CD4-FITC).

☒ The axis scales are clearly visible. Include numbers along axes only for bottom left plot of group (a 'group' is an analysis of identical markers).

☒ All plots are contour plots with outliers or pseudocolor plots.

☒ A numerical value for number of cells or percentage (with statistics) is provided.

Methodology

Sample preparation: For human samples, primary tumor or tumor draining lymph node samples were maintained in Hank's Balanced Salt solution until processing. Samples were then cut into small pieces, digested with a collagenase/liberase enzyme cocktail, and homogenized using a MACS Dissociator. Digested tumors were then washed with buffer through a 70um filter into a single cell suspension. Samples were then lysed using red blood cell ACK lysis buffer, followed by a 44% Percoll/RPMI gradient. Single cell suspensions were then either used fresh or frozen in freezing media (FBS + 10%DMSO) at -80C for future use.

For mouse samples: Tumors, lymph nodes, spleens and lungs were harvested and digested in Collagenase D (2mg/mL) shaking for 25 mins at 37C. Inguinal and axillary lymph nodes on the side of tumor inoculation were pooled as tumor draining lymph nodes (TDLNs). All digested tissues were washed with RPMI supplemented with 2%FBS through a 0.7um filter into single cell suspension. Tumors and spleen were RBC lysed and resuspended in FACS buffer. Tumors went through a 10 min 44% Percoll/RPMI gradient for 10 mins to remove excess fat prior to staining. Livers went through a 44% and 67% Percoll gradient for 20 mins to remove excess fat and hepatocytes.

Instrument: Flow cytometry data were collected on a Symphony instrument A5 with FACSDiva software v9.0 (BD).

Software: Flow cytometry data were analyzed on Flowjo v10.7.1(TreeStar) and statistical analysis was performed on Prism v9.00 (GraphPad).

Cell population abundance: The manuscript presents the frequency and number of all cell populations measured in all experiments.

Gating strategy: Refer to Extended Data Figure 11 for gating strategies for human and mouse experiments.

☒ Tick this box to confirm that a figure exemplifying the gating strategy is provided in the Supplementary Information.